Title: The hippocampus supports deliberation during value based decisions

Authors: Akram Bakkour[1,*], Daniela J. Palombo[2,§], Ariel Zylberberg[3-5], Yul H.R. Kang[3,¶], Allison Reid[2], Mieke Verfaellie[2], Michael N. Shadlen[3-5], Daphna Shohamy[1,5]

Affiliations:

[1]Department of Psychology, Columbia University, New York, NY 10027, USA.

[2]Memory Disorders Research Center, VA Boston Healthcare System and Boston University School of Medicine, Boston, MA 02130, USA.

[3]Department of Neuroscience, Columbia University, New York, NY 10027, USA.

[4]Howard Hughes Medical Institute.

[5]Mortimer B. Zuckerman Mind Brain Behavior Institute and The Kavli Institute for Brain Science, Columbia University, New York, NY 10027, USA.

[§]Current address: Department of Psychology, The University of British Columbia, Vancouver, BC V6T 1Z4, Canada.

[¶]Current address: Computational and Biological Learning Lab, Department of Engineering, University of Cambridge, Cambridge CB2 1PZ, UK.

***Correspondence**: ab4096@columbia.edu.

Abstract

Choosing between two items involves deliberation and comparison of the features of each item and its value. Such decisions take more time when choosing between options of similar value, possibly because these decisions require more evidence, but the mechanisms involved are not clear. We propose that the hippocampus supports deliberation about value, given its well-known role in prospection and relational cognition. We assessed the role of the hippocampus in deliberation in two experiments. First, using fMRI in healthy participants, we found that BOLD activity in the hippocampus increased as a function of deliberation time. Second, we found that patients with hippocampal damage exhibited more stochastic choices and longer reaction times than controls, possibly due to their failure to construct value based on internal evidence during deliberation. Both sets of results were stronger in value-based decisions compared to perceptual decisions.

Keywords: *decision making; memory; hippocampus; fMRI; Amnesia*

Introduction

Some decisions involve more deliberation than others. Even seemingly simple decisions such as those that involve preferences between a pair of familiar items take more time when they involve a choice between options of similar subjective value. This simple observation holds across many kinds of decisions, whether they are based on perception of the environment—is the apple green or red? (Cassey, Evens, Bogacz, Marshall, & Ludwig, 2013; Gold & Shadlen, 2007; Ratcliff, 2002; Usher & McClelland, 2001)—or on internal values and preferences—do I prefer a green apple or a red one? (Basten, Biele, Heekeren, & Fiebach, 2010; Hunt et al., 2012; Krajbich, Armel, & Rangel, 2010; Milosavljevic, Malmaud, Huth, Koch, & Rangel, 2010). One explanation for why such decisions take more time is that a commitment to a choice depends on the accumulation of evidence to a threshold, and when the evidence is weaker, more samples are required to reach such a threshold (Krajbich et al., 2010; Milosavljevic et al., 2010). This idea has been studied extensively in perceptual decisions about dynamic stimuli (e.g. moving dots) for which more time clearly provides more samples of external evidence, and therefore can improve the accuracy of the decision (Britten, Newsome, Shadlen, Celebrini, & Movshon, 1996; Britten, Shadlen, Newsome, & Movshon, 1993; Hanks et al., 2015; Mazurek, Roitman, Ditterich, & Shadlen, 2003; Newsome & Paré, 1988; Salzman, Britten, & Newsome, 1990). It is less clear why the same framework would apply to value-based decisions, which depend on internal evidence (Krajbich et al., 2010; Milosavljevic et al., 2010). In such cases, it is not known what the source of the evidence is and why more samples should be required to decide between options that are close in value.

We sought to understand the processes involved in deliberation when making value-based decisions. Our central hypothesis is that the hippocampus plays a key role in this deliberation

process, contributing to the comparison between items and the construction of internal samples of evidence bearing on the decision.

This hypothesis is guided by several observations. First, extensive research demonstrates that the hippocampus is necessary for detailed and vivid prospection about future events (Addis & Schacter, 2008; Buckner, 2010; Hassabis, Kumaran, Vann, & Maguire, 2007; Klein, Loftus, & Kihlstrom, 2002; Race, Keane, & Verfaellie, 2011; Schacter, Addis, & Buckner, 2007). This sort of prospection is likely to guide value-based decisions because it allows a decision-maker to imagine the detailed outcome of each choice option. Second, and more broadly, the hippocampus is known to contribute to relational encoding (Cohen & Eichenbaum, 1993; Horner & Burgess, 2013), a term coined by Cohen and Eichenbaum (1993) to capture the essential role of the hippocampus across many cognitive processes that involve flexible comparison and association between distinct items and features (for reviews, see Barry & Maguire, 2019; Davachi, 2006; Eichenbaum, 2000; 2018; Konkel & Cohen, 2009; Palombo, Keane, & Verfaellie, 2015a; Shohamy & Turk-Browne, 2013). This relational function of the hippocampus is thought to underlie its well-known role in episodic memory, but the comparison of multiple dimensions of items and their relation to each other is also likely to help guide deliberation during decision making by supplying internal evidence about each option. Recent studies have indeed linked hippocampal-based mnemonic processes to choice behavior by demonstrating that the hippocampus is involved in decisions that explicitly depend on memory by requiring participants to use novel associations acquired in the experiment (Barron, Dolan, & Behrens, 2013; Gluth, Sommer, Rieskamp, & Büchel, 2015; Wimmer & Shohamy, 2012). However, a critical open question remains about whether the hippocampus also contributes to seemingly simple decisions—between two highly familiar items—without the explicit demand to use memory.

We conducted two experiments to address this question. First, we conducted an fMRI study in healthy young participants while they made decisions based on well-established subjective value (fMRI; Experiment 1). We reasoned that if the hippocampus supports deliberation, then longer decision times should be related to more engagement of the hippocampus. Second, to test whether the hippocampus plays a causal role in resolving value-based decisions, we tested amnesic patients with damage to the hippocampus and surrounding medial temporal lobe (MTL) as well as age-, education-, and verbal IQ-matched healthy controls (Patients; Experiment 2). Although a choice between two familiar items is not typically thought to depend on the hippocampal memory system (Bartra, McGuire, & Kable, 2013; Padoa-Schioppa & Assad, 2006; Platt & Plassmann, 2014; Rangel & Clithero, 2014; Rangel, Camerer, & Montague, 2008), we reasoned that amnesic patients may nonetheless show differences in the way they deliberate about simple value-based decisions. Amnesic patients could take *less time* because their decisions involve less deliberation, or they could take *more time* because they try unsuccessfully to deliberate using evidence derived from relational mechanisms. In the latter case, the extra time would not improve their decisions.

In both experiments, participants performed a *value-based decision* task in which they made a series of choices between two familiar food items (**Figure 1**). The subjective value of each individual item was determined for each participant using an auction procedure in advance (see *Methods*), so that we could systematically vary the difference in value between the two items (i.e. $\Delta Value$) during the decision task (see also Grueschow, Polania, Hare, & Ruff, 2015; Krajbich et al., 2010; Milosavljevic et al., 2010; Polania, Moisa, Opitz, Grueschow, & Ruff, 2015). The same participants also took part in a control condition in which they made *perceptual decisions* about the dominant color of a dynamic random dot display (**Figure 1** and **Figure 1—video 1**). The perceptual comparison task solicits the same choice and reaction time behavior but is based on external sensory input.

In Experiment 1, we found that decision time in the value-based decision task was longer when the choice options were closer in value, as expected (Krajbich et al., 2010; Milosavljevic et al., 2010; Polania et al., 2015). We also found that reaction times correlated with hippocampal BOLD activity, and this effect was localized to regions of the hippocampus that showed activity related to memory retrieval, independently identified in the same participants. In Experiment 2, we found that amnesic patients were somewhat more stochastic and much slower when making value-based decisions. Importantly, despite parallel behavioral findings in value-based decisions and perceptual decisions in the healthy controls, both the hippocampal BOLD effects and the impairments in patients were selective to the value-based decision task. Together, these findings establish a critical role for the hippocampus in value-based decisions about familiar choice options.

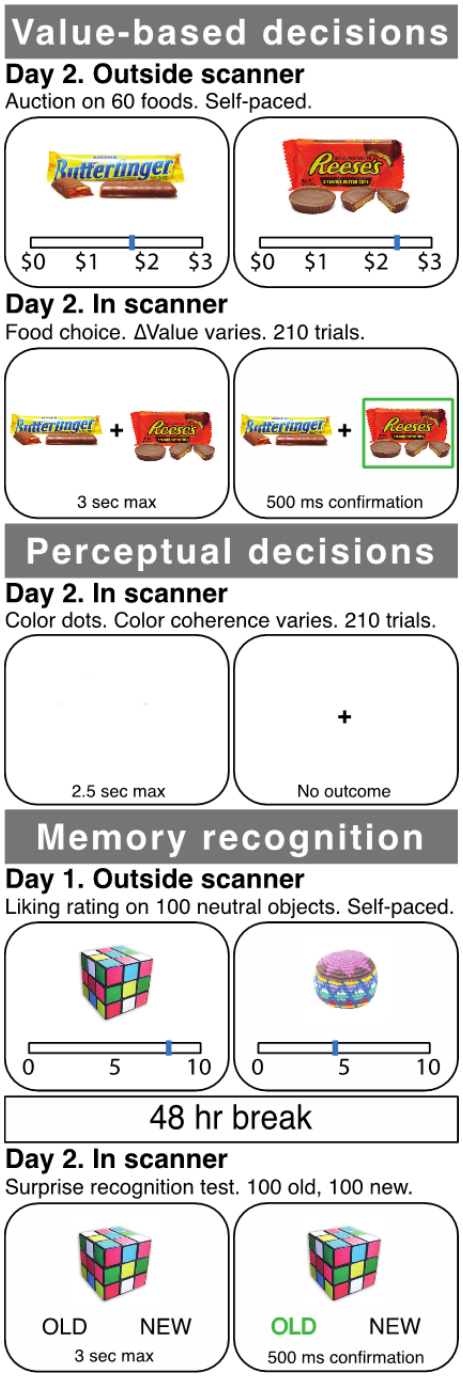

Figure 1: Experimental tasks. In Experiment 1, healthy participants were scanned with fMRI during three different tasks: a value-based decision task (top), a perceptual decision task (middle), and a memory recognition task (bottom). **In the value-based decision task**, participants were presented with 150 pairs of foods that differed on Δ*Value* (based on a pre-task auction procedure for rating the items; see *Methods*). Participants were told to choose the item that they preferred and that their choice on a randomly selected trial would be honored at the end of the experiment. **In the perceptual decision task**, participants were presented with 210 trials of a cloud of flickering blue and yellow dots that varied in the proportion of blue versus yellow (color coherence). Participants were told to determine whether the display was more blue or more yellow. **In the recognition memory localizer task**, participants underwent a standard recognition task using incidental encoding of everyday objects: first, they rated 100 objects (outside of the scanner); 48 hours later they were presented with a surprise memory test in the scanner, in which 'old' objects were intermixed with 100 'new' objects, one at a time, and participants were asked to indicate whether each object was 'old' or 'new'. In Experiment 2, amnesic patients with MTL damage and healthy controls performed variants of the value-based and perceptual decision tasks (see *Methods*).

Results

We conducted two experiments to test the mechanisms underlying deliberation in value-based decisions. In the first experiment, we scanned healthy young participants with functional MRI while they performed value-based and perceptual decision tasks. In the second experiment, we tested behavior in amnesic patients with damage to the hippocampus and surrounding MTL as well as age-, education-, and verbal IQ-matched healthy control participants on slightly modified versions of these two decision tasks (see *Methods*).

Experiment 1: Functional MRI

Behavior in both decision tasks conforms to sequential sampling models

On the perceptual decision task, healthy young participants (n = 30) made more accurate decisions when the color was more biased toward blue or yellow (**Figure 2A**, top) and reaction times (RT) were longer for decisions between options that were more difficult to discriminate (i.e. color coherence near zero, **Figure 2A**, bottom). Similarly, on the value-based decision task, participants made decisions more consistent with their subjective valuation when $\Delta Value$ was larger (**Figure 2B**, top). RTs were longer for decisions between options for which the magnitude of $\Delta Value$ ($|\Delta Value|$) was smaller (**Figure 2B**, bottom). For both the perceptual and the value-based tasks, choices and RT were well-described by drift diffusion models (**Figure 2**, solid lines). This observation is consistent with prior work (Krajbich, Hare, Bartling, Morishima, & Fehr, 2015; Ratcliff & McKoon, 2008; Shadlen & Kiani, 2013) and with the proposal that both types of decisions arise through a process of sequential sampling that stops when the accumulation of evidence satisfies a threshold or bound. The choice functions and range of RT were comparable in the two tasks, as were the goodness of fits (for model parameter estimates, see **Figure 2—source data 1**; for individual participant fits, see **Figure 2—figure supplement**

1). Some of the differences between the fits, apparent by eye, are attributed to the different scales of evidence strength in the two tasks (see **Figure 2—figure supplement 2**). We considered simpler parameterizations of the model, but the full model presented here produced a better fit compared to a model with no power law (BIC = 19.45), and a better fit compared to a model with no power law and flat bounds (BIC = 168.45).

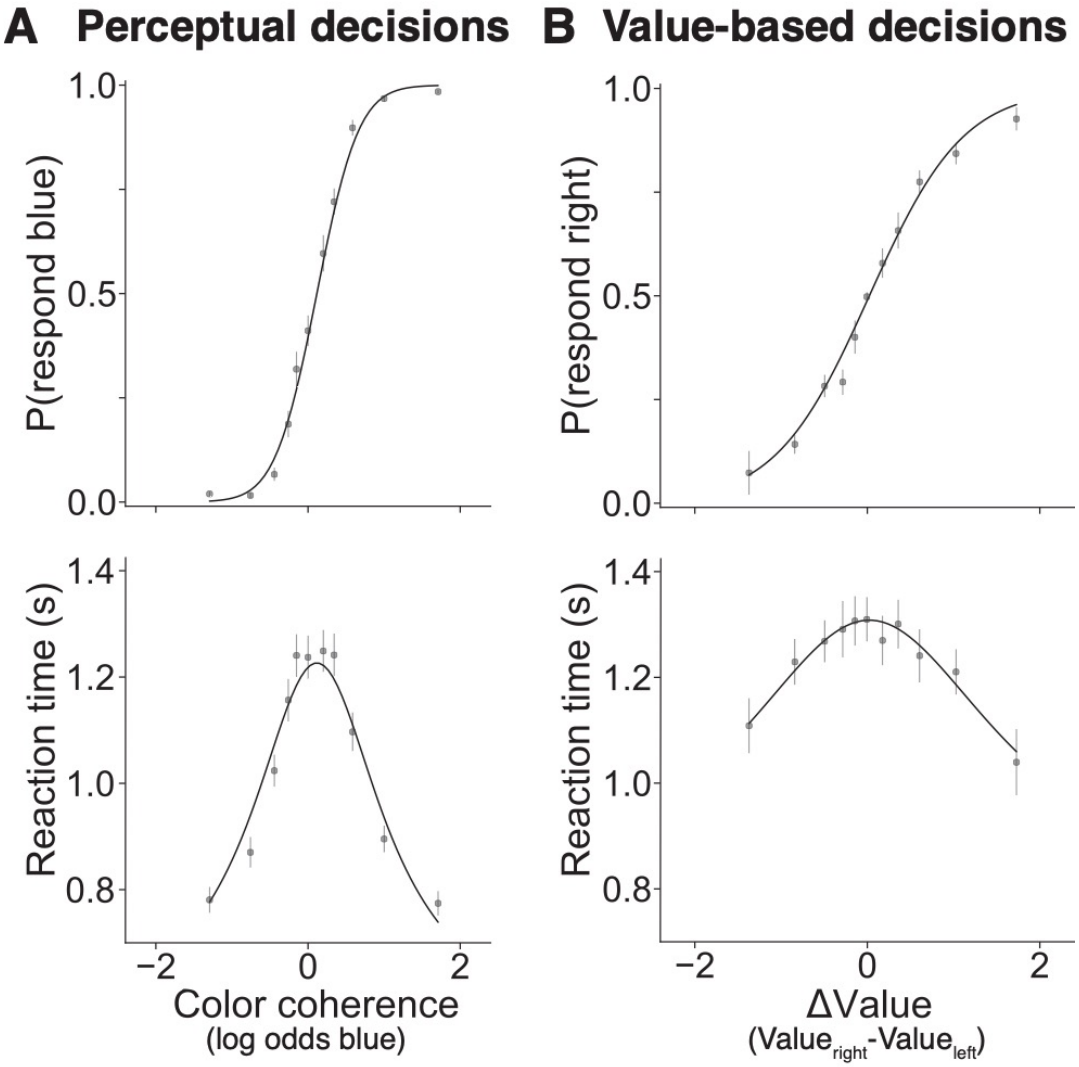

Figure 2: Choices between options that are similar take more time for both perceptual and value-based decisions in Experiment 1. Behavioral results from 30 young healthy participants for (**A**) perceptual and (**B**) value-based decisions. **A)** Proportion of blue choices (top) and mean RT (bottom) plotted as a function of signed color coherence (the logarithm of the odds that a dot is plotted as blue). **B)** Proportion of right item preference (top) and mean RT (bottom) plotted as a function of value difference (the subjective value of the item on the right side of the screen minus the subjective value of the item on the left) binned into eleven levels. Gray symbols are means (error bars are s.e.m.); solid black lines are fits to drift diffusion models. See **Figure 2—figure supplement 1** for fits to data from individual participants. See **Figure 2—figure supplement 3** for parameter recovery analysis.

Timing of value-based decisions is related to brain correlates of memory

We first conducted a whole-brain analysis to identify regions in the brain that show (*i*) an effect of RT: a correlation between RT and BOLD activity for the value-based task more so than for the perceptual task, and (*ii*) a memory effect: greater BOLD activity for successful retrieval of object memories (using the separate object-memory localizer task, see *Methods*, **Figure 3—figure supplement 1** and **Figure 3—source data 2**). Each of these analyses of the fMRI data (RT; memory retrieval) identified largely separate networks of brain regions (**Figure 3—figure supplement 1** and **Figure 3—figure supplement 3**, Stark & Squire, 2001; Yarkoni, Barch, Gray, Conturo, & Braver, 2009). Critically, however, both showed significant effects in the hippocampus and, as shown in **Figure 3** (and **Figure 3—source data 1**), the *conjunction* of these two effects revealed significant shared BOLD activity in the hippocampus. BOLD activity in memory-related hippocampal regions was more positively correlated with RT for value-based decisions than perceptual decisions, consistent with our hypothesis that deliberation associated with resolving preference relies on memory-related hippocampal mechanisms.

We conducted a series of control analyses to consider possible alternative explanations for the differential hippocampal activation on value-based versus perceptual tasks. First, the hippocampal BOLD activity might be related simply to the fact that the value-based decision task makes more demands on memory because it depends on identifying objects. Indeed, a main effect of value-based versus perceptual decisions reveals differences in BOLD activity along the ventral stream and in the medial temporal lobe, including the hippocampus (**Figure 3—figure supplement 2A** and **Figure 3—source data 3**). However, if object identification were the reason for the RT effects, one would expect to find only a main effect of task—that is, an overall difference between the two tasks regardless of deliberation time—rather than a significant interaction between task and RT. The observation of both a main effect of task and an interaction with RT suggests that differences in object recognition do not account for the

finding in the hippocampus. Second, we wondered whether the hippocampal BOLD activity in the value-based task could be related to the fact that for some participants there was a difference in the range of RT in the value-based task compared to the perceptual task. To test this, we repeated the analysis using only trials that shared the same range of RT on the two tasks (by participant). This analysis revealed a similar result (**Figure 3—figure supplement 2B** and **Figure 3—source data 4**), suggesting that the difference in the hippocampus is not related to differences in RT range.

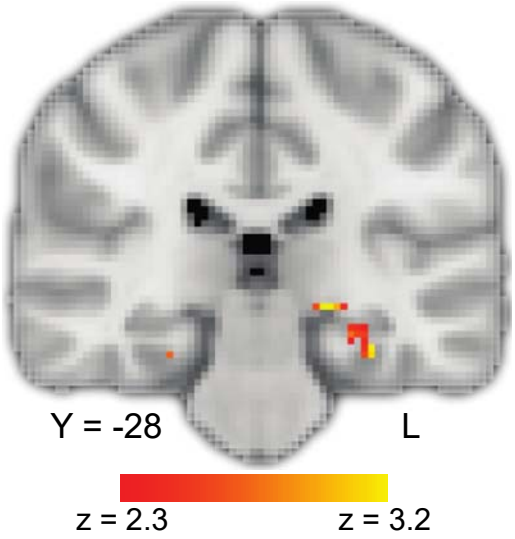

Figure 3: Deliberation time during value-based decisions is related to activation in the hippocampus. The figure shows a representative slice at the level of the hippocampus. The map exploits all three tasks and shows a comparison of the effect of trial-by-trial RT on value-based decisions with perceptual decisions, localized (with a conjunction analysis) to regions of the brain that also show a memory-retrieval effect. The full map can be viewed at https://neurovault.org/collections/BOWMEEOR/images/56727. This effect in the hippocampus was replicated with a separate analysis controlling for potential confounds (e.g. mean value across items in a pair; **Figure 3—figure supplement 3D**). Coordinates reported in standard MNI space. Heatmap color bars range from z-stat = 2.3 to 3.2. The map was cluster corrected for familywise error rate at a whole-brain level with an uncorrected cluster-forming threshold of z = 2.3 and corrected extent threshold of $p < 0.05$.

A third possibility we considered was that the tasks differ in overall levels of difficulty. Indeed, RT is a function of the difficulty levels in each of the two tasks, but there is also variability in RT within each level of difficulty, allowing us to address questions about RT while controlling for difficulty. Therefore, we tested the possibility that difficulty accounted for more of the variance in

hippocampal BOLD activity than RT by repeating the same analysis as in **Figure 3** while controlling for the magnitude of color coherence and $\Delta Value$, as well as other potential correlates of RT (e.g. mean of the pair of values; see *Methods*). This analysis again revealed RT-related activity in the hippocampus that is greater for value-based than perceptual decisions, even after accounting for other correlates of RT, both within an anatomical ROI of bilateral hippocampus and at a whole-brain corrected level (**Figure 3—figure supplement 3** and **Figure 3—source data 5-8**). The conjunction between the RT effect and the memory map was again found within the hippocampus ROI (**Figure 3—figure supplement 3H**). Finally, because our memory encoding task involved value judgments (see methods), we reran the conjunction analysis using an independent memory recognition localizer that was not specific to value-based encoding, instead using two independent meta-analysis maps from neurosynth.org based on the terms “autobiographical memory” and “recollection”. The three-way conjunction between the differential effect of RT on BOLD and these two meta-analysis maps also shows overlap in the hippocampus (**Figure 3—figure supplement 4**).

Connectivity between hippocampus and parietal cortex increases with value-based decision time

The fMRI results suggest that BOLD activity in the hippocampus is related to the time it takes to make value-based decisions. We next explored the broader neural circuits that interact with the hippocampus during value-based decisions and how activity in such circuits varies with RT. We used a psychophysiological interaction (PPI) analysis to identify brain regions with activity that covaried in an RT-dependent manner with the activity of hippocampal “seed” voxels—i.e. those that exhibited RT-dependent activation on the value-based decision task and memory-related activation on the memory localizer task. The strongest RT-dependent correlation was between the hippocampus and the parietal cortex (superior parietal lobule and precuneus), showing that

functional connectivity between the hippocampus and parietal cortex was greater for value-based decisions that took longer (**Figure 4 and Figure 4—source data 1)**.

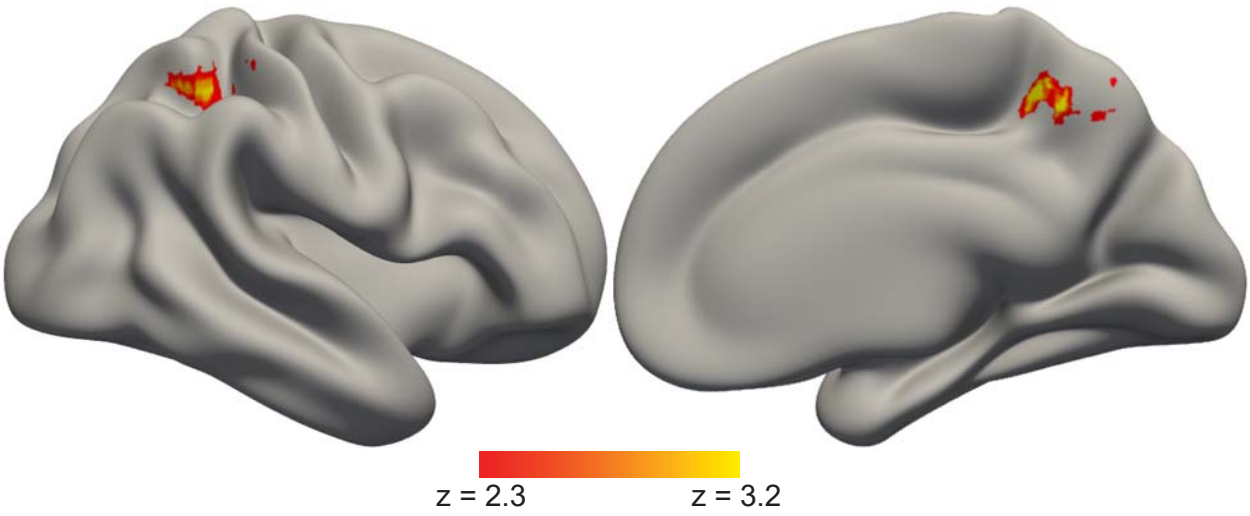

Figure 4: Timing of value-based decisions is related to functional coupling between the hippocampus and parietal cortex. Lateral (left) and medial (right) view of a semi-inflated surface of a template brain. PPI results were projected onto the cortical surface. There was a stronger correlation in activity between the hippocampus and the parietal cortex when value-based decisions took more time. The full map can be viewed at https://neurovault.org/collections/BOWMEEOR/images/129376. Heatmap color bars range from z-stat = 2.3 to 3.2. The map was cluster corrected for familywise error rate at a whole-brain level with an uncorrected cluster-forming threshold of z = 2.3 and corrected extent of $p < 0.05$.

Experiment 2: Behavior in amnesic patients

The fMRI data reveal that the timing of value-based decisions is related to BOLD activity in the hippocampus, suggesting a possible role for the hippocampus in the deliberation process. However, fMRI can only tell us about brain activity correlated with a mental process, leaving open the critical question of whether the hippocampus plays a direct, causal role in value-based decisions. Experiment 2 was designed to address this question by testing value-based decision making in patients with amnesia subsequent to damage to the hippocampus and nearby MTL structures.

Our overarching hypothesis is that the hippocampus contributes to value-based decisions by supporting the comparison of options, the simulation of outcomes, and the recollection of internal evidence. We therefore expected that damage to the hippocampus would impair this deliberation process. As noted earlier, we had no strong prediction regarding whether patients would show faster or slower RTs in general. We reasoned that slower RTs might reflect efforts to search for evidence to resolve decisions, whereas faster RTs might reflect choices that lack deliberative reasoning altogether. Patients with hippocampal damage are not known to have general impairments in valuation processes and the experiment only included food items that each patient fully recognized (see *Methods*). Therefore, we expected that patients would make choices largely consistent with their subjective valuations. Finally, for the perceptual task, we expected the patients to show intact performance, consistent with the notion that the hippocampus is not needed to make decisions based on external evidence.

Timing of value-based decisions is impaired in amnesic patients

We tested six amnesic patients with damage to the hippocampus and surrounding MTL on the decision tasks from Experiment 1, slightly modified to accommodate the patient population (see *Methods*). The patients have well-characterized memory impairments combined with intact verbal reasoning and IQ (see **Table 1**), and have participated in several prior studies (Foerde, Race, Verfaellie, & Shohamy, 2013; Grilli & Verfaellie, 2016; Palombo, Di Lascio, Howard, & Verfaellie, 2018; Palombo, Keane, & Verfaellie, 2015b). We compared the patients to fourteen age-, education-, and verbal IQ-matched healthy participants.

Table 1: Amnesic patient demographic and neuropsychological data.

Patient #	Diagnosis	Gender	Age	Edu	WAIS III		WMS III			BNT	FAS	L-N Sequence	years since onset
					VIQ	WMI	GM	VD	AD				
P01	Hypoxic-ischemic	F	67	12	88	75	52	56	55	-1.3	-1.1	-2	27.29
P02	Status epilepticus + left temp. lobectomy	M	54	16	93	94	49	53	52	-4.6	-0.96	-1	29.17
P03	Hypoxic-ischemic	M	61	14	106	115	59	72	52	0.54	-0.78	1.33	24.18
P04	Hypoxic-ischemic	M	65	17	131	126	86	78	86	1.3	0.03	1.33	15.00
P05	Encephalitis	M	75	13	99	104	49	56	58	-0.11	-0.5	0.33	5.85
P06	Stroke	M	53	20	111	99	60	65	58	1.02	2.1	-0.33	3.45

Age in years at first session; Edu, education in years; WAIS-III, Wechsler Adult Intelligence Scale-III (Wechsler, 1997a); WMS-III, Wechsler Memory Scale-III (Wechsler, 1997b); VIQ, verbal IQ; WMI, working memory index; GM, general memory; VD, visual delayed; AD, auditory delayed; scores are age-adjusted such that a score of 100 is the age-adjusted mean with a standard deviation of 15; BNT, Boston Naming Test; FAS, verbal fluency test; L-N, Letter-Number Sequence. BNT, FAS and L-N scores were z-scored against normative data for each test.

On the perceptual decision task, both patients and healthy participants made more accurate decisions when the color was more strongly biased toward blue or yellow (**Figure 5A**, top). The RTs of both the patients and healthy participants were longer for decisions between options that were more difficult to discriminate (i.e., color coherence near zero, **Figure 5A**, bottom). Patients took about the same amount of time as healthy controls to make a perceptual decision and there were no significant differences between the groups on accuracy (i.e. slopes of the choice function in **Figure 5A**, $p = 0.28$) or RT (interaction between |color coherence| and group on RT, $p = 0.18$; and main effect of group on RT, $p = 0.41$). Further, for both groups, choices and RTs were well-described by a drift diffusion model (**Figure 5A**, solid lines), suggesting that damage to the hippocampus did not impair the patients' ability to make decisions that require sequential sampling of external evidence.

In contrast, on the value-based decision task the amnesic patients' performance diverged from that of healthy controls. Although the amnesic patients' choices were clearly governed by

321 Δ*Value* (red sigmoid function, **Figure 5B** top, simple effect of *ΔValue* on choices among
322 amnesics, $p < 0.0001$), their choices were more stochastic than those of the controls (flatter red
323 sigmoid function, **Figure 5B** top, $p = 0.0008$). This observation implies that the amnesic patients
324 were not randomly guessing or forgetting the subjective value of the items but were less
325 sensitive to their difference. Notably, the patients did not show any obvious differences in their
326 use of the value rating scale nor in the resulting range of *ΔValues* (**Figure 5—figure**
327 **supplement 3**). This implies that the flatter choice function is not explained by a difference in
328 the use of the value rating scale but that the Δ*Value* derived from that scale had less purchase
329 on their choices.
330
331 The more striking difference between the two groups was observed on RT during value-based
332 decisions: the amnesic patients were substantially slower than healthy controls (**Figure 5B**
333 bottom, $p = 0.0004$). These slower RTs were specific to the value-based compared to the
334 perceptual decision task ($p = 0.002$ for the interaction between task type and group on RT). In
335 addition, their RTs were less driven by subjective value ratings (flatter red curve in **Figure 5B**
336 bottom). This difference between amnesic patients and healthy controls was statistically reliable
337 ($p = 0.015$, interaction between $|\Delta Value|$ and group on RT in a mixed effects linear regression,
338 see *Methods*). In principle, slower decisions could be a sign of a speed-accuracy tradeoff
339 favoring accuracy, but that does not appear to be the case, as the patients were both slower
340 and less accurate (i.e., less consistent with initial subjective values) than the controls. To clarify
341 this point, we calculated an index of efficiency (I_E) for each participant (average accuracy
342 divided by the average RT). The index captures the extent to which additional time was used to
343 resolve sources of uncertainty that contribute to stochastic choice behavior. For perceptual
344 decisions, I_E did not differ between amnesic patients and healthy controls (**Figure 5C**, $t_{17.21} =$
345 0.02, $p = 0.98$, Welch's t-test), presumably because the uncertainty originates in the stimulus
346 and its noisy representation by sensory neurons (Britten et al., 1993; Mante, Sussillo, Shenoy, &

Newsome, 2013; Shadlen & Newsome, 1998). For value-based decisions, I_E was significantly lower in the amnesic patients compared to controls (**Figure 5D**, $t_{11.84} = 4.2$, $p = 0.0007$, Welch's t-test). This implies that whatever deliberative process the amnesics engaged in to reach their decisions, it was less efficient than the process used by the controls.

To further characterize differences in the deliberative process between the groups, we evaluated an alternative to the drift-diffusion model. In this "heuristic model", the decision maker makes (1) fast choices for items they like strongly, (2) fast choices for an item paired with one they dislike strongly, and (3) slow stochastic choices when the preference is not resolved by rules 1 and 2 (see *Methods* and **Figure 5—figure supplement 4**). The model is representative of a class of alternatives that would account for RT and choice based on distinct rules—that is, a break from sequential sampling with optional stopping. While we found no support for this model in healthy controls (DDM performs better than this heuristic model, BIC = 537.5), at least one feature of the RTs from the amnesic patients is consistent with this model (**Figure 5—figure supplement 4**). This observation does not provide definitive support for the heuristic above, but it does suggest that the measurable differences between amnesics and controls in accuracy and RT may be related to a fundamental difference in how the amnesics resolve value-based preferences.

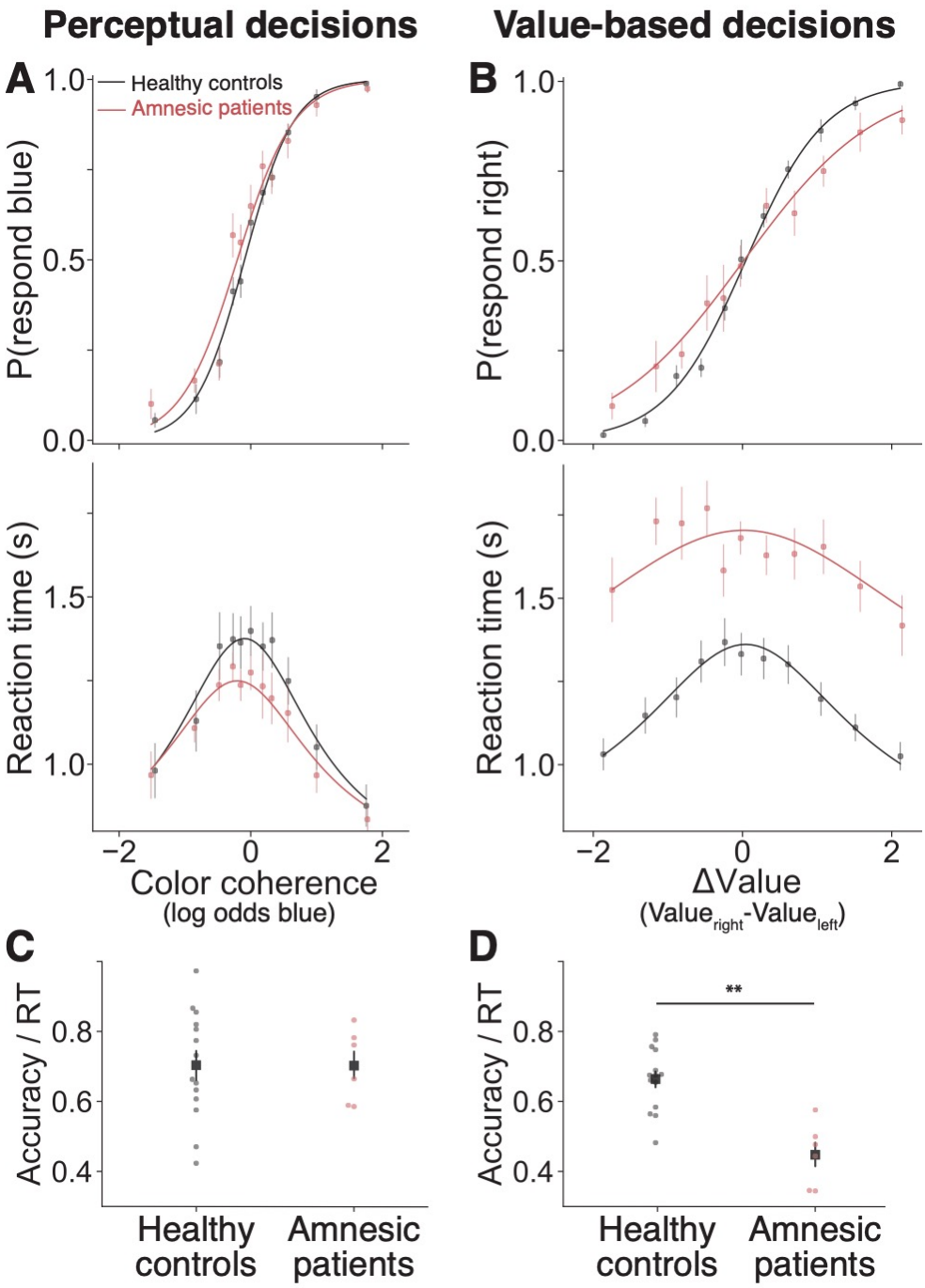

Figure 5: Amnesic patients exhibited more stochastic choices and longer reaction times on value-based decisions but not perceptual decisions. A) Proportion of blue choices (top) and mean RT (bottom) plotted as a function of signed color coherence, the logarithm of the odds that a dot is plotted as blue. Data from 14 healthy controls and 6 amnesic patients (2922 and 1246 trials, respectively). **B**) Proportion of right-item preference (top) and mean RT (bottom) plotted as a function of value difference (right minus left) binned into eleven levels. Data from 14 healthy controls and 6 amnesic patients (2893 and 1118 trials, respectively). To further summarize these findings, we plot individual average speed-adjusted accuracy, calculated as average accuracy divided by average RT per participant during (**C**) perceptual decisions and (**D**) value-based decisions (here, accuracy is defined as choices that are consistent with the individuals' initial value ratings). Circle symbols are data from amnesic patients (red) and healthy age-matched controls (black). Square symbols are group averages. Error bars are s.e.m. Curves are fits of a bounded drift diffusion model (see *Methods*). See **Figure 5—figure supplement 1** for fits to data from individual participants, **Figure 5—source data 1** for model parameters fit to data from individual participants, and **Figure 5—figure supplement 4** for consideration of an alternative model.

Discussion

We found converging evidence from fMRI and patients pointing to a role for the hippocampus in deliberation between choice options in value-based decisions. In healthy participants, the time it took to resolve choices between two options was longer for near-value decisions and was correlated with BOLD activity in the hippocampus. Amnesic patients with damage to the hippocampus were just as fast as healthy controls to make perceptual decisions but took almost twice as much time to make value-based decisions. The additional time did not lead to better accuracy; in fact, the patients' choices were less accurate (i.e., more stochastic, relative to the values they initially assigned to the items). Together, these findings link the timing of value-based decisions about highly familiar options to the hippocampus.

Value-based decisions between highly familiar choice options are typically assumed to rely on subjective value (Levy & Glimcher, 2012; Rangel et al., 2008; Tversky & Kahneman, 1986). Such value signals are thought to be supported by the ventromedial prefrontal cortex (vmPFC, Camille, Griffiths, Vo, Fellows, & Kable, 2011; Fellows, 2016; Fellows & Farah, 2007; Levy & Glimcher, 2011; vmPFC, Padoa-Schioppa & Assad, 2006). Yet, even when choosing between options that differ greatly in their subjective value, such choices involve a comparison of the values by way of taking both options, their relation, and their predicted value, into account (Houston, Doan, & Roskos-Ewoldsen, 1999; Tversky, 1972; Voigt, Murawski, & Bode, 2017). Resolving the choice between two options with similar value likely requires the generation of additional information—that is, evidence—to resolve the indecision. This evidence must come from internal sources and might involve multiple dimensions of comparisons between the options. In that sense, it may seem obvious that deliberating between even highly familiar options is likely to involve the sort of relational mechanisms that the hippocampus is known to support.

Our findings suggest that the role of the hippocampus in value-based decisions is almost certainly more nuanced than memory retrieval of the value associated with each of the items. Prior work suggests that simple object-value associations do not depend on the hippocampus (Neubert, Mars, Sallet, & Rushworth, 2015; Reynolds, Hyland, & Wickens, 2001; Rudebeck et al., 2008; Rushworth, Noonan, Boorman, Walton, & Behrens, 2011; Schultz, Dayan, & Montague, 1997; Vo, Rutledge, Chatterjee, & Kable, 2014). Moreover, it is not obvious why a simple associative memory process would account for longer deliberation times. Instead, we propose that the hippocampus contributes to deliberative processes during decision making. Specifically, we propose that deliberation may be served by the construction of value from internal evidence and engagement in the comparison between the options. Such a process is likely to also involve evaluation of alternatives and prospection about future hypothetical experiences. Prior work suggests that all of these processes are likely to engage the hippocampus (Barron et al., 2013; Eichenbaum & Cohen, 2001; Schacter et al., 2007). Future work will be necessary to evaluate how these different processes interact and whether their unique contributions may differ under different circumstances.

Our findings extend recent results demonstrating a role for the hippocampus in value-based decisions under conditions in which value information has been experimentally manipulated to depend on retrieval of new associative memories (Barron et al., 2013; Gluth et al., 2015; Wimmer & Shohamy, 2012). Recent work has also characterized sampling processes during value-based decisions that are reliant on memory (Bornstein & Norman, 2017; Bornstein, Khaw, Shohamy, & Daw, 2017; Duncan & Shohamy, 2016). Our study builds on these findings to implicate the hippocampus functionally and establish a causal role for the hippocampus in decisions about familiar options for which value is known. One open question is whether this role varies as a function of the nature of the items under deliberation. For example, natural

versus packaged items may vary in the extent to which perceptual features reveal their value; the color of an apple is revealing of its sweetness, the color of a package of chocolate perhaps less so. But ultimately, all such decisions depend on the transformation of external perceptual input to internal estimates of subjective value bearing on the relative desirability of the items. It is this deliberative process—beyond the simple item-value association—that we posit the hippocampus contributes to.

The pattern of behavior among the amnesic patients provides further insight into how and when the hippocampus is necessary for value-based decision making. We found that amnesic patients were somewhat less consistent in their decisions and that they took much longer to make them. A similar pattern has been shown recently in healthy older adults with mild memory deficits (Levin, Fiedler, & Weber, 2018). As noted earlier, it is unlikely that amnesic patients simply cannot remember the value of the items, as their choices are not arbitrary. This suggests that the patients may be relying on degraded value signals that are coarser than those in controls. Studies of simple valuation have described general valence signals in neurons in orbitofrontal cortex, striatum, amygdala, and anterior cingulate cortex that could potentially drive these choices (**Figure 3—figure supplement 5**, Hayden, Pearson, & Platt, 2009; Hikosaka, Kim, Yasuda, & Yamamoto, 2014; Padoa-Schioppa & Assad, 2006; Platt & Plassmann, 2014; R. A. Saez, Saez, Paton, Lau, & Salzman, 2017). Interestingly, patients with vmPFC damage also show greater stochasticity in their choices (Camille et al., 2011; Fellows & Farah, 2007; Pelletier & Fellows, 2019), but do not display the slowing in RT during deliberation that we see in the patients with amnesia due to hippocampal damage. This finding and others (Jones & Wilson, 2005; Wikenheiser, Marrero-Garcia, & Schoenbaum, 2017; Wimmer & Büchel, 2016), point to possible complementary roles for the hippocampus and the vmPFC in guiding value-based decisions (also see, McCormick, Ciaramelli, De Luca, & Maguire, 2018), with the

hippocampus possibly supporting evidence-based construction of value and deliberation (Weilbächer & Gluth, 2016).

If patients resolve their choices by accessing a simpler form of value representation, then why do they take such a long time to reach decisions? We propose that this reflects the patients' attempt to engage hippocampal relational mechanisms and their failure to do so. This conclusion is based on a detailed consideration of the relationship between time, accuracy, and choices. In particular, it may help to elaborate on an important difference between the decision processes at play in the value and perceptual decisions we studied. For both tasks, choice and RT were reconciled by fits to drift diffusion models, indicating that both perceptual and value-based decisions exhibit a systematic relationship in speed and accuracy as a function of difficulty. In the perceptual task, a sequence of samples of blue and yellow dots can be converted by the visual system to samples of evidence by *spatially integrating* blue or yellow (or the difference) across the stimulus aperture in sampling epochs governed by the temporal resolution of the color system, which is slower than the frame rate of the display. These samples arrive in series until the subject terminates the decision. The samples are independent, identically distributed random values drawn from a distribution with an expectation (i.e., mean) determined by the stimulus strength and a variance governed by the stochastic properties of the stimulus and the neurons that represent blue, yellow or blue minus yellow. The accumulation of these noisy samples is analogous to a deterministic drift plus diffusion.

As mentioned earlier, similar logic has been applied to value-based decisions (Krajbich & Rangel, 2011; Milosavljevic et al., 2010; Polania et al., 2015), but the analogy breaks down at the nature of the evidence samples. One might posit that neurons that represent value provide the samples of evidence (Rangel et al., 2008; Rangel & Clithero, 2014; Sokol-Hessner, Hutcherson, Hare, & Rangel, 2012). However, the stimulus provides only one sample of the

objects, and there is no reason to think that the brain would then generate a sequence of independent samples of $\Delta Value$ (Shadlen & Shohamy, 2016). Instead, we reason that the comparison itself triggers constructive thought processes to provide samples of evidence that bear on evaluation of the items along a dimension. It is hard to imagine integrating these samples of $\Delta Value$ along different dimensions, although it is possible if they were converted to some common currency (e.g., Kira, Yang, & Shadlen, 2015). It seems at least equally likely that each sample leads to a new internal estimate of preference, only to terminate if such a sample provides a sufficiently compelling preference. Although such a process involves no integration, the drift diffusion model can be fit to such a process well enough to render these alternatives indistinguishable (Ditterich, 2006). On this view, the longer RTs in the amnesic patients stem from their continued effort to generate evidence to resolve the comparison. Accordingly, the greater stochasticity in their choices possibly stems from the fact that they may fail to generate such evidence and ultimately fall back on a more rudimentary and noisier form of value representation to guide their choices. We are not committed to this specific interpretation and consider a simple heuristic strategy that accounts for some aspects of the data (see **Figure 5—figure supplement 4**).

One limitation of the present study is that we are unable to identify the specific hippocampal-based process that guides deliberation. We can only observe the manifestation of the process in RT and its associated changes in hippocampal BOLD activity or the effect of hippocampal damage. In future work, it will be useful to guide the dimensions of inquiry (e.g., saltiness) and/or construct memories associated with these dimensions that have discernible effects on BOLD activity. In this study, we deliberately avoided any possibility of biasing participants to adopt a memory-based strategy to resolve value preference, as we were interested in testing whether memory spontaneously contributed to such decisions without instruction or guidance.

The idea that memory supports construction of evidence to guide value-based decisions offers new insights to our understanding of how decisions are made, as well as the role of the hippocampus in guiding behavior. The finding that the hippocampus supports deliberation between choice options with similar subjective value addresses a challenge that has long puzzled economists and philosophers (often referred to as Buridan's paradox, Chislenko, 2016; Sorensen, 2004). By linking the hippocampus to choice behavior, this finding also highlights the pervasive and broad role of the hippocampus in guiding actions and decisions. Research on the hippocampus has typically focused on its role in supporting the formation of conscious, declarative memories for episodes of one's life. The current findings add to a growing shift in this point of view, suggesting that the hippocampus may serve a more general purpose in guiding behavior by providing behaviorally relevant input about relational associations to implicitly guide actions and decisions (Chun & Phelps, 1999; Eichenbaum & Cohen, 2001; Hannula, Ryan, Tranel, & Cohen, 2007; Olsen et al., 2016; Palombo, Keane, & Verfaellie, 2015a; Ryan, Althoff, Whitlow, & Cohen, 2000; Schapiro, Gregory, Landau, McCloskey, & Turk-Browne, 2014; Shohamy & Turk-Browne, 2013; Wimmer & Shohamy, 2012).

Materials and Methods

Human subjects

Experiment 1: young healthy fMRI participants

Thirty-three healthy participants were recruited through fliers posted on campus and the surrounding area in New York City. Three participants were excluded from analysis due to excessive motion during MRI scanning. The final sample consisted of n = 30 (19 female), mean age = 24.7 ± 5.5 and self-reported Body Mass Index (BMI) = 23 ± 4.5. No statistical method was employed to pre-determine the sample size. The sample size we chose is similar to that used in previous publications.

All experimental procedures were approved by the Institutional Review Board (IRB) at Columbia University and all scan participants provided signed informed consent before taking part in the study.

Experiment 2: amnesic patients and age-matched healthy control participants

Eight patients with amnesia due to damage to the hippocampus and sixteen age-, education- and verbal IQ-matched healthy control participants were recruited to participate in a version of the same study (for details of the differences between the scan study and the patient study, see below). Two patients and two age-matched healthy control participants were excluded; one patient and one healthy participant did not perform the perceptual decision task satisfactorily (i.e. they did not tend to choose the color that was dominant in the stimulus), one healthy participant did not perform the value-based decision task satisfactorily (i.e. their choices were not consistent with their initial preference ratings) and one patient never completed the perceptual decision task. The final sample included n = 6 patients (1 female) with amnesia (see **Table 1** for demographic and neuropsychological data) and n = 14 (6 female) healthy controls

matched for age (61.6 ± 10.5), education (15.7 ± 3.6), and verbal IQ (WAIS III VIQ = 109.5 ± 10.2). All patients presented with severe anterograde and retrograde amnesia. Patients had lower than normal memory scores (two to three standard deviations below normal as measured by WMS-III, **Table 1**), but were largely within normal range for measures of working memory and verbal aptitude. Lesions of five of the MTL patients are presented in **Figure 5—figure supplement 2**, either on MRI or CT images. The remaining patient (P04) had suffered cardiac arrest and could not be scanned due to medical contraindications. MTL pathology for this patient was inferred based on etiology and neuropsychological profile. For the patient who suffered encephalitis (P05), clinical MRI was acquired only in the acute phase of illness, with no visible lesions observed on T1-weighted images. However, T2-flair images demonstrated bilateral hyperintensities in the hippocampus and MTL cortices, as well as the anterior insula. Within the MTL, two patients (P03, P06) had lesions restricted to the hippocampus, while 3 patients had volume loss extending outside of the hippocampus (P01, P02, P05). For four of the patients (P02, P03, P05, P06), it was possible to determine that the lesion overlapped with the peak of hippocampal activation in the fMRI study. All patients and age-matched healthy participants provided informed consent in accordance with the Institutional Review Boards at Boston University and the VA Boston Healthcare System.

Tasks

Experiment 1

The study took place over two sessions. On the first day, participants were not scanned. They were trained on the perceptual color dots task (details below), received feedback (correct/incorrect) on each trial during training, and were trained to criterion, defined as 80% or higher accuracy over the last four blocks of 10 trials. Training consisted of a minimum 200 trials and a maximum 400 trials. After color dots training, participants underwent incidental encoding for the Memory Localizer task: they rated 100 neutral objects, presented one at a time on the

computer screen, on how much they liked that object by placing the cursor along a visual analog scale that ranged from 0 (least) to 10 (most) using the computer mouse. This liking rating task served as a memory encoding phase, followed two days later by a surprise memory recognition test in the scanner (details below). The first study session lasted about one hour. When it ended, participants were told to refrain from eating or drinking anything besides water for four hours before their next appointment. On the second session, which took place two days after the first session, participants took part in an auction outside of the scanner. They were then placed in the MRI scanner and performed the food choice task, the color dots task, and the memory recognition task.

Auction

Participants were endowed with $3, which they used to take part in an auction. The auction followed Becker-Degroot-Marschak (BDM) rules (Becker, Degroot, & Marschak, 1964). This auction procedure allowed us to obtain a measure of willingness-to-pay (WTP) for each of 60 appetitive food items per participant (Plassmann, O'Doherty, & Rangel, 2007). Participants were presented with one snack item at a time, in random order, on a computer screen. They placed their bid by moving a cursor on an analog scale that spanned from $0 to $3 at the bottom of the screen using the computer mouse. The auction was self-paced, and the next item was presented only after the participant placed his or her bid. After participants placed bids on all 60 items, they were given a chance to revise their bids to account for adjustments and scaling effects that can occur after participants experience the full food stimulus set. Participants were presented with each of the 60 items in random order a second time with their original bid displayed below and were asked whether they wanted to change their bid. If they clicked “NO”, they were presented with the next food item, and their original bid was kept as the WTP for that item. If participants clicked “YES”, the $0 to $3 analog scale was presented and they placed a new bid using the mouse as before. This new bid was recorded as the final WTP for that item.

The starting location of the cursor along the analog scale was randomized on each trial and the mouse cursor was reset to the middle of the screen on each trial to prevent participants from simply clicking through the entire auction phase without deliberation. Participants were told that a single trial would be drawn at random at the end of the session, and that they could bid any amount of the full $3 for each food item because the auction repeated in an independent fashion for each of the 60 items. They were told that their best strategy to win the auction was to bid exactly what each item was worth to them to purchase from the experimenter at the end of the experiment and that bidding consistently high or consistently low was a bad strategy. At the end of the session, the computer generated a counter bid in the form of a random number between $0 and $3 in increments of 25 cents. If the computer bid was higher than the participant's bid, then he or she lost the auction; if the participant matched or outbid the computer, he or she was offered to purchase the randomly drawn food item from the experimenter at the lower price generated by the computer. The outcome of the auction was played out at the end of the experimental session. After performing the auction outside the scanner, participants performed the following three tasks in the scanner while functional brain images were acquired.

Food Choice

The 60 food items were rank-ordered based on WTPs obtained during the auction, and 150 unique pairs made up from the 60 items were formed such that the difference in WTP between the two items in a pair (i.e. Δ*Value*) varied. Each of the 60 items appeared in five different pairs. Pairs were presented in random order, one pair at a time, with one item on each side of a central fixation cross. Right/left placement of the higher value item in a pair was counterbalanced across trials. Participants were instructed to choose the food they preferred. Participants chose one item on each trial by pressing one of two buttons on an MRI-compatible button box. They were given up to 3 s to make their selections. After a choice was made, the selected item was highlighted for 500 ms. If participants did not make a choice before the 3 s

cutoff, the message “Please respond faster” was displayed for 500 ms. Trials were separated by a jittered inter-trial-interval (ITI) drawn from an exponential distribution with a mean of 3, if the value generated was below 1 or above 12, it was redrawn. The true average of the resulting distribution of ITIs across trials was 3.05 s with an sd = 2.0 s. Participants were told that they would be given the chosen food on a single randomly selected trial to eat. Participants were presented with 210 trials total, split into three 70-trial scan runs. Runs of the food choice were interleaved with runs of the color dots task (below). Of the 150 unique pairs, 90 pairs were presented only once and 60 pairs were presented twice. Thus, each of the 60 food items was presented 7 times in total. Each scan run of the food choice task lasted 7 min.

Color Dots

Participants viewed a dynamic random dot display and were asked to determine whether there were more yellow or blue dots. Dots were presented at random locations within a central circular aperture (diameter 5 cm) and replaced in each video frame (60 Hz) by new dots (density 16.7 dots•cm^{-2}•s^{-1}) at new random positions. Each dot was assigned a color randomly with probability controlled by the color coherence, $C = log(p_{blue}/p_{yellow})$, such that $p_{blue} = \frac{e^C}{1+e^C}$ and $p_{yellow} = 1 - p_{blue}$. A dot that is not blue is yellow. Throughout a single trial, C was fixed at a value drawn from a set of 11 possible levels {-2, -1, -0.5, -0.25, -0.125, 0, 0.125, 0.25 0.5, 1, 2}. For C > 0 (p_{blue} > 0.5) a blue choice is graded as correct regardless of the actual ratio of blue:yellow dots displayed. For C < 0 (p_{yellow} > 0.5) a yellow choice is graded as correct regardless of the actual ratio of blue:yellow dots actually displayed. For C = 0 (p_{blue} = p_{yellow} = 0.5), the assignment of correct was deemed 0.5. The color strength is |C|.

Participants responded by pressing one of two buttons, with the color-button mapping counterbalanced across participants. Participants were instructed to make their response as

soon as they had an answer. The stimulus was presented for a maximum of 2.5 s. If they responded within the 2.5 s window, the stimulus disappeared and a central fixation cross reappeared. Intertrial intervals were generated using the same procedure used for the value-based decision task, resulting in a distribution mean across trials of 3.04 s with an sd = 2.4. Participants did not receive feedback during the main data collection, but on session 1 (training; no scanning) they received correct/incorrect feedback on each trial. Feedback appeared after a response was made and remained on the screen for 500 ms. If they did not respond within the 2.5 s choice window, a message asking participants to please respond faster was displayed for 500 ms. Participants were presented with a total of 210 trials, split into three scan runs of 70 trials each. Each scan run of the color dots task lasted 6.5 min.

Memory Recognition

Participants were presented with the 100 objects they had rated during session 1 as well as 100 new objects, randomly intermixed, one object at a time in the middle of the screen. Below the image of the object and to the right and left of center appeared the words “OLD” and “NEW” that corresponded to the right/left button mapping. On each trial, participants were asked to determine whether the object on the screen was old, meaning they remembered rating that object on their first visit or if the object was new, meaning they did not remember seeing or rating that object. Participants responded by pressing one of two buttons on an MRI-compatible button box. Old/New response-button mapping was counterbalanced across participants. The stimulus remained on the screen for a maximum of 3 s. If participants responded within the 3 s response window, their choice (i.e. OLD or NEW) was highlighted for 500 ms. If they did not respond within the 3 s window, a message asking them to please respond faster was displayed for 500 ms. Trials were separated by a jittered ITI generated using the same procedure as for the other two tasks and resulted in a distribution mean across trials of 3.0 s with an sd = 1.98 s.

676 The 200 trials were split into four scan runs of 50 trials (approximately 5 min) each. All four runs
677 of this task were consecutive, with no other intervening tasks in between.
678
679 *Experiment 2*
680 The patients and age-matched healthy participants performed a version of the scan study that
681 did not include the memory recognition task and was performed outside of the scanner. The
682 study was conducted over two days; on one day participants took part in the value-based
683 decision task and on the other day they took part in the perceptual decision task. The order in
684 which tasks were performed was counterbalanced across participants. The value-based
685 decision task differed from the task in experiment 1 in four ways. (1) The food stimuli used were
686 different and consisted of a wider range of non-packaged foods, not just snack foods. (2) Rather
687 than a BDM auction, participants indicated their pre-experimental preferences for 30 food items
688 using a preference rating scale. Participants were instructed to rate how much they prefer to eat
689 the food item on the screen from 0 (prefer least to eat) to 10 (prefer most to eat). Participants
690 were asked to name the food item on the screen before rating it. Foods that a participant did not
691 recognize or misnamed were excluded from analysis. This ensured that only familiar foods were
692 included in the analysis. Ratings were z-scored within participant and $\Delta Value$ was calculated
693 from the z-scored ratings for 210 unique pairs of items, none of which repeated during the food
694 choice task. (3) Participants were given 3.5 seconds rather than 2.5 seconds to make a choice.
695 (4) Participants were not asked to fast before the experiment and did not receive a snack at the
696 end of the experiment based on their choice on a randomly selected trial. The perceptual
697 decision task differed from the task in experiment 1 in three ways: 1) participants received only
698 40 practice trials, 2) participants continued to receive correct/incorrect feedback throughout the
699 entire task, and 3) participants were given 3.5 seconds to make a choice. Prior to the perceptual
700 task, participants were trained on selecting blue or yellow using the proper button on the
701 keyboard to ensure that they learned the color-button mapping prior to starting the perceptual

decision task. Participants were trained for only 40 trials rather than to criterion and continued to receive correct/incorrect feedback for all trials.

fMRI acquisition

Imaging data were acquired on a 3 T GE MR750 MRI scanner with a 32-channel head coil. Functional data were acquired using a T2*-weighted echo planar imaging sequence (repetition time (TR) = 2 s, echo time (TE) = 22 ms, flip angle (FA) = 70°, field of view (FOV) = 192 mm, acquisition matrix of 96 x 96). Forty oblique axial slices were acquired with a 2 mm in-plane resolution positioned along the anterior commissure-posterior commissure line and spaced 3 mm to achieve full brain coverage. Slices were acquired in an interleaved fashion. Each of the food choice runs consisted of 212 volumes, each of the color dots runs consisted of 197 volumes, and the memory test runs consisted of 150 volumes. In addition to functional data, a single three-dimensional high-resolution (1 mm isotropic) T1-weighted full-brain image was acquired using a BRAVO pulse sequence for brain masking and image registration.

Behavioral analysis

Choice and reaction time data

Choice and RT data were analyzed using regression models. Choice data were scored on accuracy (correct choice in the perceptual decision task or consistency of responses with the stated value for the choice option—WTP for the scan study and preference rating for patient study—i.e. score 1 for trials when the participant chose the food with higher WTP/rating and 0 if they chose the food with lower WTP/rating). These binary data were then entered into a repeated measures logistic regression mixed effects model to calculate the odds of choosing correctly/consistently with their prior valuation and test the relationship between choices and task difficulty (color coherence or $\Delta Value$). $\Delta Value$ for the scan study was calculated by subtracting the WTP for the item on the left side of the screen from the WTP for the item on the

right side of the screen. Δ*Value* for the patient study was calculated by subtracting the z-scored rating (z-scored within participant) for the item on the left from the z-scored rating of the item on the right. RT data were entered into a mixed effects repeated measures linear regression model to test the relationship between RT and |color coherence| or |Δ*Value*|. For the patient study, we also entered group assignment as a predictor in the models and its interaction with Δ*Value* separately for each task. For the patient study, we also ran a full model combining across both tasks to assess the three-way interaction between group (patient or healthy), task type (perceptual or value-based), and difficulty on choices or RT.

Drift diffusion model

We fit a one-dimensional drift diffusion model to the choice and RT on each decision. The model assumes that choice and RT are linked by a common mechanism of evidence accumulation, which stops when a decision variable reaches one of two bounds. The decision variable (x) is given by the cumulative sum of samples from a Normal distribution with mean μdt and variance dt,

$$dx = \mu dt + \mathcal{N}(0, dt) \quad (1)$$

Where $\mathcal{N}$ represents an independent sample from a Normal distribution with mean 0 and variance dt, that is, the increment of a Wiener process. The accumulation starts with x = 0.

In the value-based decision, the mean of the momentary evidence (also termed the drift rate) is given by

$$\mu = \kappa s|V_R - V_L|^p + \mu_0 \quad (2)$$

where V_R and V_L are the values of the right and left item respectively, κ is a fitted constant, *s* is the sign of the value difference (positive if $V_R > V_L$, negative otherwise), *p* is a fitted exponent and μ_0 implements a bias to the drift rate to account for non-symmetric distributions of choice or RT between left and right choices. If *p*=1, then κs would yield a drift rate that varies linearly as a function of Δ*Value*. The power law instantiates the possibility that the monotonic relationship between Δ*Value* and drift rate is not necessarily linear. κ, p, and μ_0 are fitted parameters.

In the color-discrimination task, the mean of the momentary evidence is given by

$$\mu = \kappa s|C|^p + \mu_0 \quad (3)$$

where C is the color coherence, and s is positive if C > 0 and negative otherwise. There is reason to expect $p \approx 1$ for the color-discrimination task, but we allowed this degree of freedom (for parity).

We used time-varying decision bounds to account for potential differences in RT between correct and error trials. This is the normative implementation of bounded drift diffusion when there are multiple difficulty levels (Drugowitsch, Moreno-Bote, Churchland, Shadlen, & Pouget, 2012). The shape of the bound was determined by three parameters. The initial bound height, B_0, remains constant for $0 \le t < B_{del}$, and then collapses exponentially towards zero with time constant B_2 (in seconds). The two bounds were assumed to be symmetrical around x = 0. For the value-based task, the positive bound represents a commitment to a right-item choice, and the negative bound represents a commitment to a left item choice. For the perceptual task, the positive and negative bounds indicate a commitment to the blue and yellow choices,

779 respectively. The RT is given by the sum of the decision time, determined by the drift-diffusion
780 process, and a non-decision time that we assume Gaussian with mean t_{nd} and standard
781 deviation σ_{tnd}.
782
783 We performed separate fits for perceptual- and value-based tasks. The model was fit to
784 maximize the joint likelihood of choice and RT of each trial. The likelihood of the parameters
785 given the data from each trial was obtained by numerically solving the Fokker-Planck (FP)
786 equation describing the dynamics of the drift-diffusion process. We used fast convolution
787 methods to find the numerical solution to the FP equation. The parameter optimization was
788 performed using the Nelder-Mead Simplex Method (Lagarias, Reeds, Wright, & Wright, 1998) to
789 minimize the negative log-likelihood of the parameters given the choice and RT data. All
790 parameters were bounded during the fitting procedure. We took the best fit parameters from one
791 hundred fits using random starting points to ensure that the optimization search did not get
792 stuck in a local minimum. For the value-based task, we reduced the number of unique drift-rates
793 by rounding $\Delta Value$ to multiples of 0.1 dollars. In **Figure 2** and **Figure 5**, we fit the models to
794 grouped data from all participants after binning $\Delta Value$ into 11 levels. These 11 levels had fixed
795 boundaries on $\Delta Value$ and were assigned the mean $\Delta Value$ of the points composing the bin.
796 This binning was intended to match the levels of $\Delta Value$ to the discrete levels of color
797 coherence. The fits for individual participants were performed on all trials (not binned) and are
798 shown in **Figure 2—figure supplement 1** and **Figure 5—figure supplement 1**. The best
799 fitting parameters for the grouped and non-grouped data are displayed in **Figure 2—source**
800 **data 1** and **Figure 5—source data 1**.
801
802 *Heuristic model*
803 We evaluated an alternative to drift-diffusion models, which obeys the following heuristic.
804 Suppose that a subset of food items are valued as either highly desirable (D^+) or highly

805 undesirable (D^-). All the other items are designated middling ($D^{\approx}$). This yields three types of
806 decisions: (i) Decisions between an item from D^+ and an item from the other categories (D^- or
807 $D^{\approx}$) are fast choices of the preferred item regardless of Δ*Value*. (ii) Decisions between an item
808 from D^- and an item from $D^{\approx}$ are fast choices of item from $D^{\approx}$ regardless of Δ*Value*. (iii)
809 Decisions between two items from the same class (both from D^+, both from D^-, or both from
810 $D^{\approx}$) are slow, regardless of Δ*Value* and they are stochastic. We allowed these stochastic
811 choices to be governed by a logistic function of Δ*Value*, although it could be argued that they
812 ought to be random. We refer to i and ii as *trivial* decisions and to iii as *non-trivial* decisions.
813 The only role of Δ*Value* is to determine the choice probabilities for the *non-trivial* decisions.
814 Importantly, it is uncoupled to the RT, which is uniformly slow for this category.
815
816 We implemented this model using the following degrees of freedom: κ_1 and κ_2 are criteria that
817 separate the ranges of value corresponding to D^-, $D^{\approx}$ and D^+; two means and two standard
818 deviations for the fast and slow RTs; and two degrees of freedom (β_0, β_1) for the logistic
819 regression relating the *non-trivial* choices to Δ*Value*. The model was fit to maximize the joint
820 likelihood of choice and RT of each trial. We used the Nelder-Mead Simplex Method (Lagarias
821 et al., 1998) to find the model's parameters that minimize the negative log-likelihood (NLL) of
822 the choice and RT data. RT_i and RT_{ii} are assumed to be generated from a normal distribution
823 with a mean $\mu_{RT\,fast}$ and a standard deviation $\sigma^2_{RT\,fast}$. RT_{iii} are assumed to be generated from
824 $\mu_{RT\,slow}$ and a standard deviation $\sigma^2_{RT\,slow}$. The NLL for *non-trivial* choices derive from a
825 Bernoulli (binomial) distribution: $-log(p[choice|, \beta_0, \beta_1])$. The NLL for *trivial* choices is not
826 properly specified. The model posits a deterministic decision rule for these trials, but the data
827 exhibit stochasticity (see insets in **Figure 5—figure supplement 4**). To avoid infinite
828 penalization during fitting, we assigned the probability p=0.99 for *trivial* choices consistent with

the rule, and 1-p for the exceptions. For model comparison statistics (e.g., BIC), we obtain p from the logistic function (derived from the *non-trivial* choices) evaluated at Max(|Δ*Value*|).

The arbitrary choice of penalty for inconsistent choices on *trivial* trials renders model comparison ill-posed. The same can be said for the implementation of a logistic choice function to account for the stochastic *non-trivial* choices. Nevertheless, we compared the heuristic model to the diffusion models by comparing the deviance of the best fits (same as BIC because the number of degrees of freedom are equal). We also implemented a version of the model that employs a "trembling hand" error for penalizing an incorrect choice on a *trivial* trial by allowing the probability p for *trivial* choices to be a free parameter. We find that the DDM model still performs better than this more permissive parametrization of the heuristic model (BIC = 425.88).

The unsatisfactory aspects of this model comparison exercise led us to pursue a more qualitative strategy. The heuristic model posits independence of RT and Δ*Value* once grouped by *trivial* or *non-trivial*, whereas sequential sampling models (e.g., diffusion) predict a dependence regardless of this grouping. We evaluated this prediction by examining the effect of |Δ*Value*| on RT, using mixed effects linear regression on combined data from the participants in the three experimental groups: imaging, amnesic patients and their age-matched controls. For the heuristic model, the designation of *trivial* vs. *non-trivial* was established from fits to each participant's data (i.e., κ_1 and κ_2). The analysis is shown in **Figure 5—figure supplement 4**.

Imaging analysis

Imaging data preprocessing

Raw imaging data in DICOM format were converted to NIFTI format and preprocessed through a standard preprocessing pipeline using the FSL package version 5 (Smith et al., 2004). Functional image time series were first aligned using the MCFLIRT tool to obtain six motion

parameters that correspond to the x, y, z translation and rotation of the brain over time. Next, the skull was removed from the T2* images using the brain extraction tool (BET) and from the high-resolution T1 images using Freesurfer (Fischl, Sereno, Tootell, & Dale, 1999; Ségonne et al., 2004). Spatial smoothing was performed using a Gaussian kernel with a full-width half maximum (FWHM) of 5 mm. Data and design matrix were high-pass filtered using a Gaussian-weighted least-squares straight line fit with a cutoff period of 100 s. Grand-mean intensity normalization of each run's entire four-dimensional data set by a single multiplicative factor was performed. The functional volumes for each participant and run were registered to the high resolution T1-weighted structural volume using a boundary-based registration method implemented in FSL5 (BBR, Greve & Fischl, 2009). The T1-weighted image was then registered to the MNI152 2 mm template using a linear registration implemented in FLIRT (12 degrees of freedom). These two registration steps were concatenated to obtain a functional-to-standard space registration matrix.

Food choice

We conducted a generalized linear model (GLM) analysis on the food choice task data. The first analysis included three regressors of interest: (i) onsets for all valid choice trials; (ii) same onsets and duration as (i) but modulated by RT; (iii) onsets for missed trials. After running this model, we ran a conjunction analysis using the output of this model and the equivalent model on the perceptual decision task data (see below) with our main memory retrieval success contrast (see memory recognition section below). The conjunction map is presented in **Figure 3**. This model was also used to generate the map in **Figure 3—figure supplement 2A**.

The second GLM analysis was designed to rule out the possibility that differences in RT range between the two tasks might account for a contrast between tasks in the effect of RT on BOLD. This model included five regressors of interest: (i) onsets for all valid choice trials with RT in the

range of overlap across the two tasks; (ii) same onsets and duration as (i) but modulated by RT; (iii) onsets for all valid choice trials with RT not in the range of overlap across the two tasks; (iv) onsets for missed trials. This model was used to generate the map in **Figure 3—figure supplement 2B**.

The third GLM model is the model we based our inferences on and included twelve regressors of interest: (i) onsets for non-repeated unique pair "correct" trials (i.e. unique pairs of items that were only presented once where choice was consistent with initial valuation during the auction meaning the chosen item had the higher WTP), modeled with a duration that equaled the average RT across all valid food choice trials and participants; (ii) same onsets and duration as (i) but modulated by $|\Delta Value|$ demeaned across these trials within each run for each participant; (iii) same onsets and duration as (i) but modulated by RT demeaned across these trials within each run for each participant; (iv-vi) similar to regressors (i-iii), but for non-repeated unique pair "incorrect" trials (i.e. unique pairs of items that were only presented once for which choice was inconsistent with initial valuation during the auction, meaning the chosen item had the lower WTP); (vii-ix) similar to regressors (i-iii), but for repeated unique pair trials (i.e. unique pairs of items that were presented twice, both "correct" and "incorrect" trials together); (x) to account for any differences in mean value across items in a pair (i.e. average WTP across both items in a pair) between trial types, we added a regressor with the onsets of all valid trials and the same duration as all other regressors, while the modulator was the demeaned average WTP across both items in a pair; (xi) to account for any differences in right/left choices between trial types, we added a regressor with the same onsets and durations as (x), while the modulator was an indicator for right/left response; (xii) onsets for missed trials. Maps from this model are presented in **Figure 3—figure supplement 3A, C, D, E, G, and H**.

In all models, we also included the six x, y, z translation and rotation motion parameters obtained from MCFLIRT, framewise displacement (FD) and RMS intensity difference from one volume to the next (DVARS, Power, Barnes, Snyder, Schlaggar, & Petersen, 2012) as confound regressors. We also modeled out volumes with FD and DVARS that exceeded a threshold of 0.5 by adding a single time point regressor for each “to-be-scrubbed” volume (Power, 2014). All regressors were entered at the first level of analysis and all (but the added confound regressors) were convolved with a canonical double-gamma hemodynamic response function. The temporal derivative of each regressor (except for the added confound regressors) was included in the model. The models were estimated separately for each participant and each run.

Color dots

The first GLM analysis included three regressors of interest: (i) onsets for all valid choice trials; (ii) same onsets and duration as (i) but modulated by RT; (iii) onsets for missed trials. After running this model, we ran a conjunction analysis using the output of this model and the equivalent model on the value-based decision task data (see above) with our main memory retrieval success contrast (see memory recognition section below). The conjunction map is presented in **Figure 3**. This model was also used to generate the map in **Figure 3—figure supplement 2A**.

The second GLM analysis evaluates the possibility that differences in RT variance between the two tasks might account for a contrast between tasks in the effect of RT on BOLD. This model included five regressors of interest: (i) onsets for all valid choice trials with RT in the range of overlap across the two tasks; (ii) same onsets and duration as (i) but modulated by RT; (iii) onsets for all valid choice trials with RT not in the range of overlap across the two tasks; (iv) onsets for missed trials. This model was used to generate the map in **Figure 3—figure supplement 2B**.

The third GLM model for the color dots task is the model that we based our inferences on and included 3 regressors for each of correct and incorrect color choice trial types: (i) onsets of correct trials (i.e. participant chose yellow when the coherence was negative and chose blue when the coherence was positive, as well as all coherence 0 trials) modeled with a duration which equaled the average RT across all valid color dots trials and participants; (ii) same onsets and durations as (i) but modulated by |color coherence| demeaned across these trials within each run for each participant; (iii) same onsets and durations as (i) but modulated by RT demeaned across these trials within each run for each participant; (iv-vi) similar to regressors (i-iii), but for incorrect trials (i.e. participant chose yellow when the coherence was positive and chose blue when the coherence was negative). Additionally, we included two other regressors: to account for any differences in right/left choices between trial types we added a regressor (vii) with the onsets of all valid color dots trials and the same duration as all other regressors (average RT across all trials and participants), while the modulator was an indicator for right/left response; finally, we included a regressor (viii) with onsets for missed trials. Maps from this model are presented in **Figure 3—figure supplement 3B, C, D, F, G, and H**.

For all models, we added the same covariates as in the food choice design matrix, including the six motion regressors described above, along with FD and DVARS as confound regressors.

Memory recognition

The GLM for the memory recognition task data included 8 regressors of interest: (i) onsets of hit trials (i.e. participant responded old when the object on the screen was old), modeled with a duration that equaled the average RT across all valid memory trials and participants; (ii) same onset and duration as (i) but modulated by liking rating for the object demeaned across these trials within each run for each participant; (iii) onsets of miss trials (i.e. participant responded

new when the object on the screen was old) modeled with the same duration as (i); (iv) same onset and duration as (iii) but modulated by liking rating for the object demeaned across these trials within each run for each participant; (v) onsets of correct rejection trials (i.e. participant responded new when the object on the screen was new) modeled with the same duration as (i); (vi) onsets of false alarm trials (i.e. participant responded old when the object on the screen was new) modeled with the same duration as (i); (vii) to account for any differences in RT between trial types we added a regressor with the onsets of all valid trials and the same duration as all other regressors (average RT across all trials and participants) while the modulator was the demeaned RT across all valid trials; (viii) onsets for missed trials. We added the same covariates as in the food choice design matrix, including the six motion regressors described above, along with FD and DVARS as confound regressors. The map for the contrast hits > correct rejections in this model is presented in **Figure 3—figure supplement 1**. This contrast was also used in the conjunction analysis presented in **Figure 3**.

Conjunction analysis

To test the spatial overlap in memory-retrieval-related brain activity and value-based-RT-related activation, we conducted a conjunction analysis between the maps presented in **Figure 3—figure supplement 1** (memory retrieval success contrast of hits [regressor (i) in memory recognition fMRI GLM model] greater than correct rejections [regressor (v) in memory recognition fMRI GLM model]) and the same map as in **Figure 3—figure supplement 3C**, but for the simpler model (contrast of value-based RT [regressor (iii) in the first food choice fMRI GLM model] greater than perceptual RT [regressor (iii) in the first color dots fMRI GLM model]). The conjunction map is presented in **Figure 3**.

Psychophysiological interaction (PPI)

As the seed for the PPI analysis, we used significant voxels for the contrast value-based RT greater than perceptual RT (**Figure 3—figure supplement 3C**) that lay within an anatomical mask of bilateral hippocampus (Harvard-Oxford Atlas). The PPI regressor was created by deconvolving the seed to obtain an estimated neural signal during value-based decisions using SPM's deconvolution algorithm (Gitelman, Penny, Ashburner, & Friston, 2003), calculating the interaction with the task in the neural domain and then reconvolving to create the final regressor. We followed McLaren et al.'s (McLaren, Ries, Xu, & Johnson) gPPI modeling procedure and included 9 regressors in our GLM: (i) onsets of all valid food choicelower-than-median RT trials, modeled with a duration that equaled the average RT across all valid trials and participants; (ii) onsets of all valid trials, modeled with the same duration as in i and modulated by RT; (iii) onsets of all valid trials, modeled with the same duration as in i and modulated by $|\Delta Value|$, demeaned across these trials within each run for each participant; (iv) same onsets and duration as i but modulated by the value of the chosen food, demeaned across these trials within each run for each participant; (v) to account for any differences in right/left choices, we added a regressor with the same onsets and duration as i but modulated by an indicator for right/left response; (vi) onsets of all missed trials with the same duration as i; (vii) the raw time course extracted from the seed (after registering the seed to the native space of each run for each participant); (viii) a PPI regressor with the same onsets as i. The PPI that varied linearly with RT during food choice trials generated the map in **Figure 4**.

GLM model estimation and correction for multiple comparisons

All GLM models were estimated using FSL's FEAT. The first-level time-series GLM analysis was performed for each run per participant using FSL's FILM. The first-level contrast images were then combined across runs per participant using fixed effects. The group-level analysis was performed using FSL's mixed effects modeling tool FLAME1 (Beckmann, Jenkinson, & Smith, 2003). Group-level maps were corrected to control the familywise error rate in one of two

ways: for whole-brain correction, we used cluster-based Gaussian random field correction for multiple comparisons, with an uncorrected cluster-forming threshold of $z = 2.3$ and corrected extent threshold of $p < 0.05$. For small volume correction, we used a voxel-based Gaussian random field theory-based maximum height thresholding with a voxel-level corrected threshold of $p < 0.05$ within a 3D mask of a region of interest.

Data and software availability

Data from this study are available from the corresponding author upon request. Task code and analysis code is available at https://github.com/abakkour/MDMRT_scan. Imaging analysis code is available from the corresponding author upon request.

Acknowledgements

This research was funded by the McKnight Memory and Cognitive Disorders Award (D.S.), National Science Foundation Directorate for Social, Behavioral & Economic Sciences Postdoctoral Research Fellowship grant #1606916 (A.B.), National Institutes of Health grant R01EY011378 and Howard Hughes Medical Institute (M.N.S.), VA Senior Research Career Scientist Award (MV), VA Merit Grant CX001748 (MV), National Eye Institute grant T32 EY013933 (Y.H.R.K).

The authors would like to thank Daniel Kimmel, Danique Jeurissen, and David Barack for feedback on an earlier draft of the manuscript and helpful discussions. The authors would also like to thank Lucy Owen, Sean Raymond, Eileen Hartnett, and the New York State Psychiatric Institute MR Unit staff for help with data collection. The contents of this manuscript do not represent the view of the US Department of Veterans Affairs or the US Government.

Competing interests

The authors declare no competing interests.

References

Addis, D. R., & Schacter, D. L. (2008). Constructive episodic simulation: temporal distance and detail of past and future events modulate hippocampal engagement. Hippocampus, 18(2), 227–237. http://doi.org/10.1002/hipo.20405

Bakkour A. 2019. MDMRT_scan. Github. https://github.com/abakkour/MDMRT_scan. 8e89da1.

Barron, H. C., Dolan, R. J., & Behrens, T. E. J. (2013). Online evaluation of novel choices by simultaneous representation of multiple memories. Nature Neuroscience, 16(10), 1492–1498. http://doi.org/10.1038/nn.3515

Barry, D. N., & Maguire, E. A. (2019). Remote memory and the hippocampus: a constructive critique. Trends in Cognitive Sciences, 23(2), 128–142. http://doi.org/10.1016/j.tics.2018.11.005

Bartra, O., McGuire, J. T., & Kable, J. W. (2013). The valuation system: a coordinate-based meta-analysis of BOLD fMRI experiments examining neural correlates of subjective value. NeuroImage, 76, 412–427. http://doi.org/10.1016/j.neuroimage.2013.02.063

Basten, U., Biele, G., Heekeren, H. R., & Fiebach, C. J. (2010). How the brain integrates costs and benefits during decision making. Proceedings of the National Academy of Sciences of the United States of America, 107(50), 21767–21772. http://doi.org/10.1073/pnas.0908104107

Becker, G. M., Degroot, M. H., & Marschak, J. (1964). Measuring utility by a single-response sequential method. Behavioral Science, 9(3), 226–232. http://doi.org/10.1002/bs.3830090304

Beckmann, C. F., Jenkinson, M., & Smith, S. M. (2003). General multilevel linear modeling for group analysis in FMRI. NeuroImage, 20(2), 1052–1063. http://doi.org/10.1016/S1053-8119(03)00435-X

Bornstein, A. M., & Norman, K. A. (2017). Reinstated episodic context guides sampling-based decisions for reward. Nature Neuroscience, 20(7), 997–1003. http://doi.org/10.1038/nn.4573

Bornstein, A. M., Khaw, M. W., Shohamy, D., & Daw, N. D. (2017). Reminders of past choices bias decisions for reward in humans. Nature Communications, 8, 15958. http://doi.org/10.1038/ncomms15958

Britten, K. H., Newsome, W. T., Shadlen, M. N., Celebrini, S., & Movshon, J. A. (1996). A relationship between behavioral choice and the visual responses of neurons in macaque MT. Visual Neuroscience, 13(1), 87–100.

Britten, K. H., Shadlen, M. N., Newsome, W. T., & Movshon, J. A. (1993). Responses of neurons in macaque MT to stochastic motion signals. Visual Neuroscience, 10(6), 1157–1169.

1066 Buckner, R. L. (2010). The role of the hippocampus in prediction and imagination. Annual
1067 Review of Psychology, 61(1), 27–48– C1–8.
1068 http://doi.org/10.1146/annurev.psych.60.110707.163508

1069 Camille, N., Griffiths, C. A., Vo, K., Fellows, L. K., & Kable, J. W. (2011). Ventromedial frontal
1070 lobe damage disrupts value maximization in humans. Journal of Neuroscience, 31(20), 7527–
1071 7532. http://doi.org/10.1523/JNEUROSCI.6527-10.2011

1072 Cassey, T. C., Evens, D. R., Bogacz, R., Marshall, J. A. R., & Ludwig, C. J. H. (2013). Adaptive
1073 sampling of information in perceptual decision-making. PloS One, 8(11), e78993.
1074 http://doi.org/10.1371/journal.pone.0078993

1075 Chislenko, E. (2016). A solution for Buridan's ass. Ethics, 126(2), 283–310.
1076 http://doi.org/10.1086/683537

1077 Chun, M. M., & Phelps, E. A. (1999). Memory deficits for implicit contextual information in
1078 amnesic subjects with hippocampal damage. Nature Neuroscience, 2(9), 844–847.
1079 http://doi.org/10.1038/12222

1080 Cohen, N. J., & Eichenbaum, H. (1993). Memory, Amnesia, and the Hippocampal System.
1081 Cambridge, MA: MIT Press.

1082 Davachi, L. (2006). Item, context and relational episodic encoding in humans. Current Opinion
1083 in Neurobiology, 16(6), 693–700. http://doi.org/10.1016/j.conb.2006.10.012

1084 Ditterich, J. (2006). Stochastic models of decisions about motion direction: behavior and
1085 physiology. Neural Networks, 19(8), 981–1012. http://doi.org/10.1016/j.neunet.2006.05.042

1086 Drugowitsch, J., Moreno-Bote, R., Churchland, A. K., Shadlen, M. N., & Pouget, A. (2012). The
1087 cost of accumulating evidence in perceptual decision making. Journal of Neuroscience, 32(11),
1088 3612–3628. http://doi.org/10.1523/JNEUROSCI.4010-11.2012

1089 Duncan, K. D., & Shohamy, D. (2016). Memory states influence value-based decisions. Journal
1090 of Experimental Psychology - General, 145(11), 1420–1426. http://doi.org/10.1037/xge0000231

1091 Eichenbaum, H. (2000). A cortical-hippocampal system for declarative memory. Nature Reviews
1092 Neuroscience, 1(1), 41–50. http://doi.org/10.1038/35036213

1093 Eichenbaum, H. (2018). What Versus Where: Non-spatial Aspects of Memory Representation
1094 by the Hippocampus. Current Topics in Behavioral Neurosciences, 37(8), 101–117.
1095 http://doi.org/10.1007/7854_2016_450

1096 Eichenbaum, H., & Cohen, N. J. (2001). From Conditioning to Conscious Recollection: Memory
1097 Systems of the Brain. New York: Oxford University Press.

1098 Fellows, L. K. (2016). The Neuroscience of Human Decision-Making Through the Lens of
1099 Learning and Memory. In R. E. Clark & S. Martin (Eds.), Behavioral Neuroscience of Learning
1100 and Memory (2nd ed., Vol. 37, pp. 231–251). Cham: Springer.
1101 http://doi.org/10.1007/7854_2016_468

1102 Fellows, L. K., & Farah, M. J. (2007). The role of ventromedial prefrontal cortex in decision
1103 making: judgment under uncertainty or judgment per se? Cerebral Cortex, 17(11), 2669–2674.
1104 http://doi.org/10.1093/cercor/bhl176

1105 Fischl, B., Sereno, M. I., Tootell, R. B. H., & Dale, A. M. (1999). High-resolution intersubject
1106 averaging and a coordinate system for the cortical surface. Human Brain Mapping, 8(4), 272–
1107 284.

1108 Foerde, K., Race, E., Verfaellie, M., & Shohamy, D. (2013). A role for the medial temporal lobe
1109 in feedback-driven learning: evidence from amnesia. Journal of Neuroscience, 33(13), 5698–
1110 5704. http://doi.org/10.1523/JNEUROSCI.5217-12.2013

1111 Gitelman, D. R., Penny, W. D., Ashburner, J., & Friston, K. J. (2003). Modeling regional and
1112 psychophysiologic interactions in fMRI: the importance of hemodynamic deconvolution.
1113 NeuroImage, 19(1), 200–207. http://doi.org/10.1016/S1053-8119(03)00058-2

1114 Gluth, S., Sommer, T., Rieskamp, J., & Büchel, C. (2015). Effective connectivity between
1115 hippocampus and ventromedial prefrontal cortex controls preferential choices from memory.
1116 Neuron, 86(4), 1078–1090. http://doi.org/10.1016/j.neuron.2015.04.023

1117 Gold, J. I., & Shadlen, M. N. (2007). The neural basis of decision making. Annual Review of
1118 Neuroscience, 30(1), 535–574. http://doi.org/10.1146/annurev.neuro.29.051605.113038

1119 Greve, D. N., & Fischl, B. (2009). Accurate and robust brain image alignment using boundary-
1120 based registration. NeuroImage, 48(1), 63–72. http://doi.org/10.1016/j.neuroimage.2009.06.060

1121 Grilli, M. D., & Verfaellie, M. (2016). Experience-near but not experience-far autobiographical
1122 facts depend on the medial temporal lobe for retrieval: Evidence from amnesia.
1123 Neuropsychologia, 81, 180–185. http://doi.org/10.1016/j.neuropsychologia.2015.12.023

1124 Grueschow, M., Polania, R., Hare, T. A., & Ruff, C. C. (2015). Automatic versus Choice-
1125 Dependent Value Representations in the Human Brain. Neuron, 85(4), 874–885.
1126 http://doi.org/10.1016/j.neuron.2014.12.054

1127 Hanks, T. D., Kopec, C. D., Brunton, B. W., Duan, C. A., Erlich, J. C., & Brody, C. D. (2015).
1128 Distinct relationships of parietal and prefrontal cortices to evidence accumulation. Nature,
1129 520(7546), 220–223. http://doi.org/10.1038/nature14066

1130 Hannula, D. E., Ryan, J. D., Tranel, D., & Cohen, N. J. (2007). Rapid onset relational memory
1131 effects are evident in eye movement behavior, but not in hippocampal amnesia. Journal of
1132 Cognitive Neuroscience, 19(10), 1690–1705. http://doi.org/10.1162/jocn.2007.19.10.1690

Hassabis, D., Kumaran, D., Vann, S. D., & Maguire, E. A. (2007). Patients with hippocampal amnesia cannot imagine new experiences. Proceedings of the National Academy of Sciences of the United States of America, 104(5), 1726–1731. http://doi.org/10.1073/pnas.0610561104

Hayden, B. Y., Pearson, J. M., & Platt, M. L. (2009). Fictive reward signals in the anterior cingulate cortex. Science, 324(5929), 948–950. http://doi.org/10.1126/science.1168488

Hikosaka, O., Kim, H. F., Yasuda, M., & Yamamoto, S. (2014). Basal ganglia circuits for reward value-guided behavior. Annual Review of Neuroscience, 37(1), 289–306. http://doi.org/10.1146/annurev-neuro-071013-013924

Horner, A. J., & Burgess, N. (2013). The associative structure of memory for multi-element events. Journal of Experimental Psychology - General, 142(4), 1370–1383. http://doi.org/10.1037/a0033626

Houston, D. A., Doan, K., & Roskos-Ewoldsen, D. (1999). Negative political advertising and choice conflict. Journal of Experimental Psychology. Applied, 5(1), 3–16. http://doi.org/10.1037/1076-898X.5.1.3

Hunt, L. T., Kolling, N., Soltani, A., Woolrich, M. W., Rushworth, M. F. S., & Behrens, T. E. J. (2012). Mechanisms underlying cortical activity during value-guided choice. Nature Neuroscience, 15(3), 470–6– S1–3. http://doi.org/10.1038/nn.3017

Jones, M. W., & Wilson, M. A. (2005). Theta rhythms coordinate hippocampal-prefrontal interactions in a spatial memory task. PLoS Biology, 3(12), e402. http://doi.org/10.1371/journal.pbio.0030402

Kira, S., Yang, T., & Shadlen, M. N. (2015). A neural implementation of Wald's sequential probability ratio test. Neuron, 85(4), 861–873. http://doi.org/10.1016/j.neuron.2015.01.007

Klein, S., Loftus, J., & Kihlstrom, J. (2002). Memory and temporal experience: the effects of episodic memory loss on an amnesic patient's ability to remember the past and imagine the future. Social Cognition.

Konkel, A., & Cohen, N. J. (2009). Relational memory and the hippocampus: representations and methods. Frontiers in Neuroscience, 3(2), 166–174. http://doi.org/10.3389/neuro.01.023.2009

Krajbich, I., & Rangel, A. (2011). Multialternative drift-diffusion model predicts the relationship between visual fixations and choice in value-based decisions. Proceedings of the National Academy of Sciences of the United States of America, 108(33), 13852–13857. http://doi.org/10.1073/pnas.1101328108

Krajbich, I., Armel, K. C., & Rangel, A. (2010). Visual fixations and the computation and comparison of value in simple choice. Nature Neuroscience, 13(10), 1292–1298. http://doi.org/10.1038/nn.2635

Krajbich, I., Hare, T., Bartling, B., Morishima, Y., & Fehr, E. (2015). A common mechanism underlying food choice and social decisions. PLoS Computational Biology, 11(10), e1004371. http://doi.org/10.1371/journal.pcbi.1004371

Lagarias, J. C., Reeds, J. A., Wright, M. H., & Wright, P. E. (1998). Convergence properties of the Nelder-Mead simplex method in low dimensions. SIAM Journal on Optimization, 9(1), 112–147. http://doi.org/10.1137/S1052623496303470

Levin, F., Fiedler, S., & Weber, B. (2018). The influence of episodic memory decline on value-based choice. Aging, Neuropsychology, and Cognition, 1–22. http://doi.org/10.1080/13825585.2018.1509939

Levy, D. J., & Glimcher, P. W. (2011). Comparing apples and oranges: using reward-specific and reward-general subjective value representation in the brain. Journal of Neuroscience, 31(41), 14693–14707. http://doi.org/10.1523/JNEUROSCI.2218-11.2011

Levy, D. J., & Glimcher, P. W. (2012). The root of all value: a neural common currency for choice. Current Opinion in Neurobiology, 22(6), 1027–1038. http://doi.org/10.1016/j.conb.2012.06.001

Mante, V., Sussillo, D., Shenoy, K. V., & Newsome, W. T. (2013). Context-dependent computation by recurrent dynamics in prefrontal cortex. Nature, 503(7474), 78–84. http://doi.org/10.1038/nature12742

Mazurek, M. E., Roitman, J. D., Ditterich, J., & Shadlen, M. N. (2003). A role for neural integrators in perceptual decision making. Cerebral Cortex, 13(11), 1257–1269.

McCormick, C., Ciaramelli, E., De Luca, F., & Maguire, E. A. (2018). Comparing and contrasting the cognitive effects of hippocampal and ventromedial prefrontal cortex damage: a review of human lesion studies. Neuroscience, 374, 295–318. http://doi.org/10.1016/j.neuroscience.2017.07.066

McLaren, D. G., Ries, M. L., Xu, G., & Johnson, S. C. (2012). A generalized form of context-dependent psychophysiological interactions (gPPI): a comparison to standard approaches. NeuroImage, 61(4), 1277–1286. http://doi.org/10.1016/j.neuroimage.2012.03.068

Milosavljevic, M., Malmaud, J., Huth, A., Koch, C., & Rangel, A. (2010). The Drift Diffusion Model can account for the accuracy and reaction time of value-based choices under high and low time pressure. Judgment and Decision Making, 5(6), 437–449. http://doi.org/10.2139/ssrn.1901533

Neubert, F.-X., Mars, R. B., Sallet, J., & Rushworth, M. F. S. (2015). Connectivity reveals relationship of brain areas for reward-guided learning and decision making in human and monkey frontal cortex. Proceedings of the National Academy of Sciences of the United States of America, 112(20), E2695–E2704. http://doi.org/10.1073/pnas.1410767112

Newsome, W. T., & Paré, E. B. (1988). A selective impairment of motion perception following lesions of the middle temporal visual area (MT). Journal of Neuroscience, 8(6), 2201–2211.

Olsen, R. K., Sebanayagam, V., Lee, Y., Moscovitch, M., Grady, C. L., Rosenbaum, R. S., & Ryan, J. D. (2016). The relationship between eye movements and subsequent recognition: Evidence from individual differences and amnesia. Cortex, 85, 182–193. http://doi.org/10.1016/j.cortex.2016.10.007

Padoa-Schioppa, C., & Assad, J. A. (2006). Neurons in the orbitofrontal cortex encode economic value. Nature, 441(7090), 223–226. http://doi.org/10.1038/nature04676

Palombo, D. J., Di Lascio, J. M., Howard, M. W., & Verfaellie, M. (2018). Medial temporal lobe amnesia is associated with a deficit in recovering temporal context. Journal of Cognitive Neuroscience, 1–13. http://doi.org/10.1162/jocn_a_01344

Palombo, D. J., Keane, M. M., & Verfaellie, M. (2015a). How does the hippocampus shape decisions? Neurobiology of Learning and Memory, 125, 93–97. http://doi.org/10.1016/j.nlm.2015.08.005

Palombo, D. J., Keane, M. M., & Verfaellie, M. (2015b). The medial temporal lobes are critical for reward-based decision making under conditions that promote episodic future thinking. Hippocampus, 25(3), 345–353. http://doi.org/10.1002/hipo.22376

Pelletier, G., & Fellows, L. K. (2019). A critical role for human ventromedial frontal lobe in value comparison of complex objects based on attribute configuration. Journal of Neuroscience, 2969–18. http://doi.org/10.1523/JNEUROSCI.2969-18.2019

Plassmann, H., O'Doherty, J., & Rangel, A. (2007). Orbitofrontal cortex encodes willingness to pay in everyday economic transactions. Journal of Neuroscience, 27(37), 9984–9988. http://doi.org/10.1523/JNEUROSCI.2131-07.2007

Platt, M. L., & Plassmann, H. (2014). Multistage valuation signals and common neural currencies. In P. W. Glimcher & E. Fehr (Eds.), Neuroeconomics (pp. 237–258). Academic Press. http://doi.org/10.1016/B978-0-12-416008-8.00013-9

Polania, R., Moisa, M., Opitz, A., Grueschow, M., & Ruff, C. C. (2015). The precision of value-based choices depends causally on fronto-parietal phase coupling. Nature Communications, 6, 8090. http://doi.org/10.1038/ncomms9090

Power, J. D. (2014). Statistical improvements in functional magnetic resonance imaging analyses produced by censoring high-motion data points. Human Brain Mapping, 35(5), 1981–1996. http://doi.org/10.1002/hbm.22307

Power, J. D., Barnes, K. A., Snyder, A. Z., Schlaggar, B. L., & Petersen, S. E. (2012). Spurious but systematic correlations in functional connectivity MRI networks arise from subject motion. NeuroImage, 59(3), 2142–2154. http://doi.org/10.1016/j.neuroimage.2011.10.018

Race, E., Keane, M. M., & Verfaellie, M. (2011). Medial temporal lobe damage causes deficits in episodic memory and episodic future thinking not attributable to deficits in narrative construction. Journal of Neuroscience, 31(28), 10262–10269. http://doi.org/10.1523/JNEUROSCI.1145-11.2011

Rangel, A., & Clithero, J. A. (2014). The computation of stimulus values in simple choice. In P. W. Glimcher & E. Fehr (Eds.), Neuroeconomics (pp. 125–148). Academic Press. http://doi.org/10.1016/B978-0-12-416008-8.00008-5

Rangel, A., Camerer, C., & Montague, P. R. (2008). A framework for studying the neurobiology of value-based decision making. Nature Reviews Neuroscience, 9(7), 545–556. http://doi.org/10.1038/nrn2357

Ratcliff, R. (2002). A diffusion model account of response time and accuracy in a brightness discrimination task: fitting real data and failing to fit fake but plausible data. Psychonomic Bulletin & Review, 9(2), 278–291.

Ratcliff, R., & McKoon, G. (2008). The diffusion decision model: theory and data for two-choice decision tasks. Neural Computation, 20(4), 873–922. http://doi.org/10.1162/neco.2008.12-06-420

Reynolds, J. N., Hyland, B. I., & Wickens, J. R. (2001). A cellular mechanism of reward-related learning. Nature, 413(6851), 67–70. http://doi.org/10.1038/35092560

Rudebeck, P. H., Behrens, T. E., Kennerley, S. W., Baxter, M. G., Buckley, M. J., Walton, M. E., & Rushworth, M. F. S. (2008). Frontal cortex subregions play distinct roles in choices between actions and stimuli. Journal of Neuroscience, 28(51), 13775–13785. http://doi.org/10.1523/JNEUROSCI.3541-08.2008

Rushworth, M. F. S., Noonan, M. P., Boorman, E. D., Walton, M. E., & Behrens, T. E. (2011). Frontal cortex and reward-guided learning and decision-making. Neuron, 70(6), 1054–1069. http://doi.org/10.1016/j.neuron.2011.05.014

Ryan, J. D., Althoff, R. R., Whitlow, S., & Cohen, N. J. (2000). Amnesia is a deficit in relational memory. Psychological Science, 11(6), 454–461.

Saez, R. A., Saez, A., Paton, J. J., Lau, B., & Salzman, C. D. (2017). Distinct roles for the amygdala and orbitofrontal cortex in representing the relative amount of expected reward. Neuron, 95(1), 70–77.e3. http://doi.org/10.1016/j.neuron.2017.06.012

Salzman, C. D., Britten, K. H., & Newsome, W. T. (1990). Cortical microstimulation influences perceptual judgements of motion direction. Nature, 346(6280), 174–177. http://doi.org/10.1038/346174a0

1271 Schacter, D. L., Addis, D. R., & Buckner, R. L. (2007). Remembering the past to imagine the
1272 future: the prospective brain. Nature Reviews Neuroscience, 8(9), 657–661.
1273 http://doi.org/10.1038/nrn2213

1274 Schapiro, A. C., Gregory, E., Landau, B., McCloskey, M., & Turk-Browne, N. B. (2014). The
1275 necessity of the medial temporal lobe for statistical learning. Journal of Cognitive Neuroscience,
1276 26(8), 1736–1747. http://doi.org/10.1162/jocn_a_00578

1277 Schultz, W., Dayan, P., & Montague, P. R. (1997). A neural substrate of prediction and reward.
1278 Science, 275(5306), 1593–1599.

1279 Ségonne, F., Dale, A. M., Busa, E., Glessner, M., Salat, D., Hahn, H. K., & Fischl, B. (2004). A
1280 hybrid approach to the skull stripping problem in MRI. NeuroImage, 22(3), 1060–1075.
1281 http://doi.org/10.1016/j.neuroimage.2004.03.032

1282 Shadlen, M. N., & Kiani, R. (2013). Decision making as a window on cognition. Neuron, 80(3),
1283 791–806. http://doi.org/10.1016/j.neuron.2013.10.047

1284 Shadlen, M. N., & Newsome, W. T. (1998). The variable discharge of cortical neurons:
1285 implications for connectivity, computation, and information coding. Journal of Neuroscience,
1286 18(10), 3870–3896.

1287 Shadlen, M. N., & Shohamy, D. (2016). Decision Making and Sequential Sampling from
1288 Memory. Neuron, 90(5), 927–939. http://doi.org/10.1016/j.neuron.2016.04.036

1289 Shohamy, D., & Turk-Browne, N. B. (2013). Mechanisms for widespread hippocampal
1290 involvement in cognition. Journal of Experimental Psychology - General, 142(4), 1159–1170.
1291 http://doi.org/10.1037/a0034461

1292 Smith, S. M., Jenkinson, M., Woolrich, M. W., Beckmann, C. F., Behrens, T. E. J., Johansen-
1293 Berg, H., et al. (2004). Advances in functional and structural MR image analysis and
1294 implementation as FSL. NeuroImage, 23 Suppl 1, S208–19.
1295 http://doi.org/10.1016/j.neuroimage.2004.07.051

1296 Sokol-Hessner, P., Hutcherson, C., Hare, T., & Rangel, A. (2012). Decision value computation
1297 in DLPFC and VMPFC adjusts to the available decision time. European Journal of
1298 Neuroscience, 35(7), 1065–1074. http://doi.org/10.1111/j.1460-9568.2012.08076.x

1299 Sorensen, R. (2004). Paradoxes of Rationality. In A. R. Mele & P. Rawling (Eds.), The Oxford
1300 Handbook of Rationality (pp. 257–275). Oxford University Press.

1301 Stark, C. E., & Squire, L. R. (2001). Simple and associative recognition memory in the
1302 hippocampal region. Learning & Memory, 8(4), 190–197. http://doi.org/10.1101/lm.40701

1303 Tversky, A. (1972). Elimination by aspects: A theory of choice. Psychological Review, 79(4),
1304 281–299. http://doi.org/10.1037/h0032955

Tversky, A., & Kahneman, D. (1986). Rational choice and the framing of decisions. Journal of Business, S251–S278.

Usher, M., & McClelland, J. L. (2001). The time course of perceptual choice: the leaky, competing accumulator model. Psychological Review, 108(3), 550–592.

Vo, K., Rutledge, R. B., Chatterjee, A., & Kable, J. W. (2014). Dorsal striatum is necessary for stimulus-value but not action-value learning in humans. Brain, 137(Pt 12), 3129–3135. http://doi.org/10.1093/brain/awu277

Voigt, K., Murawski, C., & Bode, S. (2017). Endogenous formation of preferences: Choices systematically change willingness-to-pay for goods. Journal of Experimental Psychology - Learning, Memory, and Cognition, 43(12), 1872–1882. http://doi.org/10.1037/xlm0000415

Wechsler, D. (1997a). Wechsler Adult Intelligence Scale—Third Edition (WAIS-III). In Administration and Scoring Manual. San Antonio, TX: Psychological Corporation.

Wechsler, D. (1997b). Wechsler Memory Scale—Third edition (WMS-III). In Administration and Scoring Manual. San Antonio, TX: Psychological Corporation.

Weilbächer, R. A., & Gluth, S. (2016). The interplay of hippocampus and ventromedial prefrontal cortex in memory-based decision making. Brain Sciences, 7(1), 4. http://doi.org/10.3390/brainsci7010004

Wikenheiser, A. M., Marrero-Garcia, Y., & Schoenbaum, G. (2017). Suppression of ventral hippocampal output impairs integrated orbitofrontal encoding of task structure. Neuron, 95(5), 1197–1207.e3. http://doi.org/10.1016/j.neuron.2017.08.003

Wimmer, G. E., & Büchel, C. (2016). Reactivation of reward-related patterns from single past episodes supports memory-based decision making. Journal of Neuroscience, 36(10), 2868–2880. http://doi.org/10.1523/JNEUROSCI.3433-15.2016

Wimmer, G. E., & Shohamy, D. (2012). Preference by association: how memory mechanisms in the hippocampus bias decisions. Science, 338(6104), 270–273. http://doi.org/10.1126/science.1223252

Yarkoni, T., Barch, D. M., Gray, J. R., Conturo, T. E., & Braver, T. S. (2009). BOLD correlates of trial-by-trial reaction time variability in gray and white matter: a multi-study fMRI analysis. PloS One, 4(1), e4257. http://doi.org/10.1371/journal.pone.0004257

Appendix 1

Experiment 1 Behavioral Results

Value-based Decisions

Participants tended to choose the item that was of higher value (as measured by willingness-to-pay in the auction phase), and this tendency increased as the value difference between the two items (i.e. Δ*Value*) increased (**Figure 2A**, top. The odds of right item choices multiplied for every \$1 increase in Δ*Value* by 5.9, 95% CI = [5.08 6.93], $p < 0.0001$). Participants' RTs increased as $|\Delta$*Value*| decreased (**Figure 2A**, bottom; $\beta = -0.11$, bootstrapped 95% CI [-0.13 -0.09], bootstrapped $p = 0.001$). These results replicate previous findings that show that choices and RTs vary systematically with Δ*Value* (Krajbich et al., 2010; Milosavljevic et al., 2010). These relationships are captured by the drift diffusion model (solid black lines in **Figure 2**), suggesting that the mechanism underlying the decision is based on accumulation of evidence.

Perceptual Decisions

When performing the color task, participants responded blue more often as the color coherence increased and responded yellow more often as the color coherence decreased (became more negative, **Figure 2B**, top. The odds of choosing blue multiplied for every unit increase of color coherence by 68.05, 95% CI [52.63 87.99], $p < 0.0001$). RTs were shortest at the lowest and highest color coherence levels. RTs were longest at color coherence level zero, when there was an equal proportion of yellow and blue dots in the stimulus (**Figure 2B**, bottom). In a repeated measures linear regression mixed effects model, |color coherence| was negatively related to RT ($\beta = -0.25$, bootstrapped 95% CI [-0.26 -0.24], bootstrapped $p = 0.001$).

Memory recognition

Participants' mean hit rate was 0.81 ± 0.15, and their mean correct rejection (CR) rate was 0.76 ± 0.15. Mean *d'* across all participants was 1.78 ± 0.57. Participants were faster when making a correct response (hits and CRs combined, mean RT = 1.24 ± 0.17) than when making an incorrect response (misses and false alarms combined, mean RT = 1.42 ± 0.24, mean of the differences in RT = 0.18, 95% CI [0.13 0.23], $t(29) = 7.07$, $p < 0.0001$). The liking ratings for objects on session 1 were related to responses and RTs during the memory recognition test on session 2. In a repeated measures logistic regression mixed effects model including only data for old objects seen on session 1, the odds of responding old multiplied for every unit increase in liking rating by 1.12 (95% CI [1.03 1.22], $p = 0.011$). In a repeated measures linear regression mixed effects model, liking rating was weakly negatively related to RT ($\beta = -0.006$, 95% CI [-0.011 -0.000], $p = 0.045$).

Figure supplements

Figure 1—video 1: Video of the colored dots stimulus. The first trial has a color coherence of 0 (equal probability that a dot is yellow or blue) and lasts for 1.44 seconds. The second trial has a color coherence of -0.125 (slightly more yellow) and lasts for 1.54 seconds.

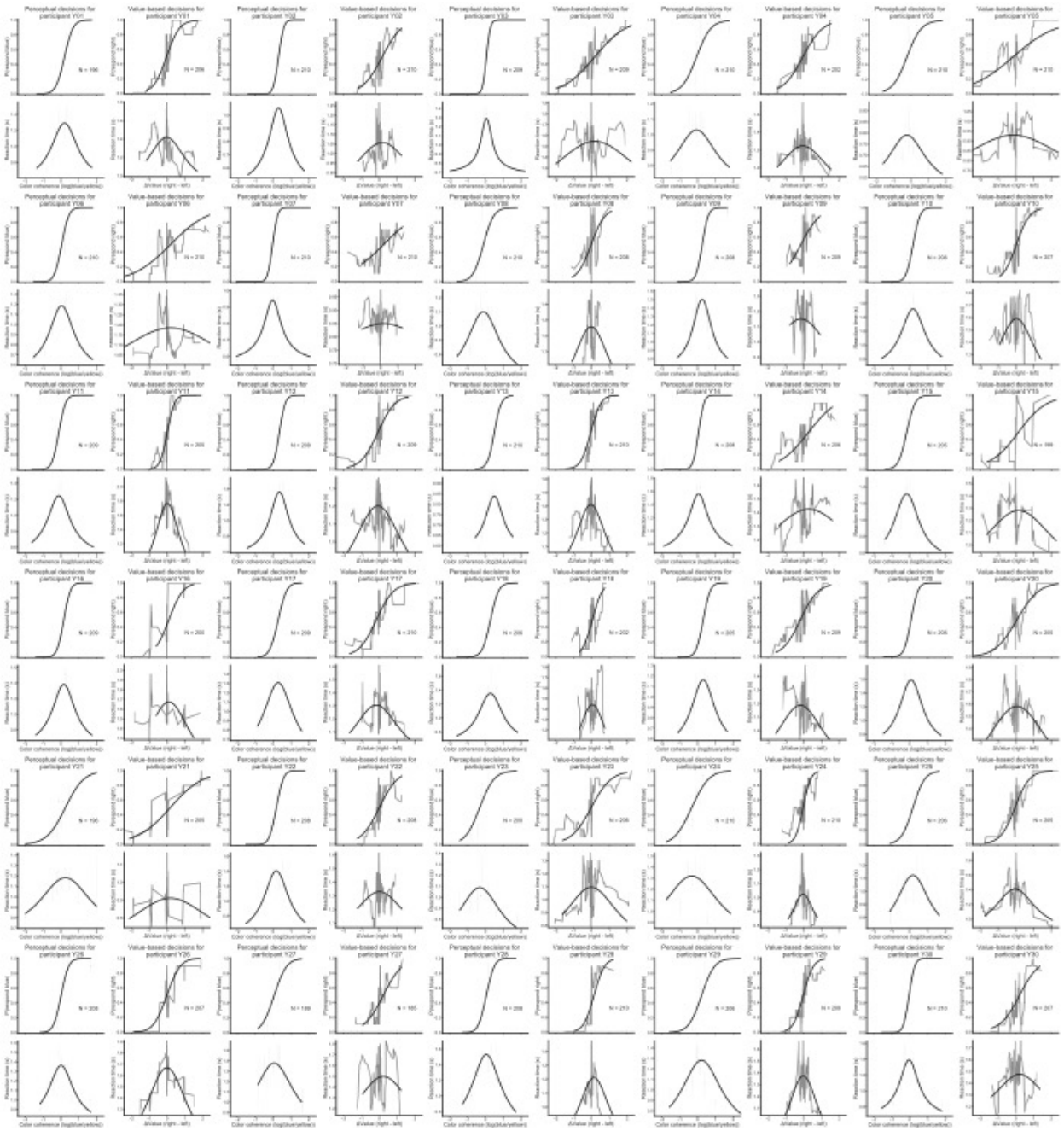

Figure 2—figure supplement 1: Data and fits for value-based and perceptual decisions per participant in Experiment 1. Light lines are running means. Dots are means and error bars are standard errors of the mean. Solid lines are model fits.

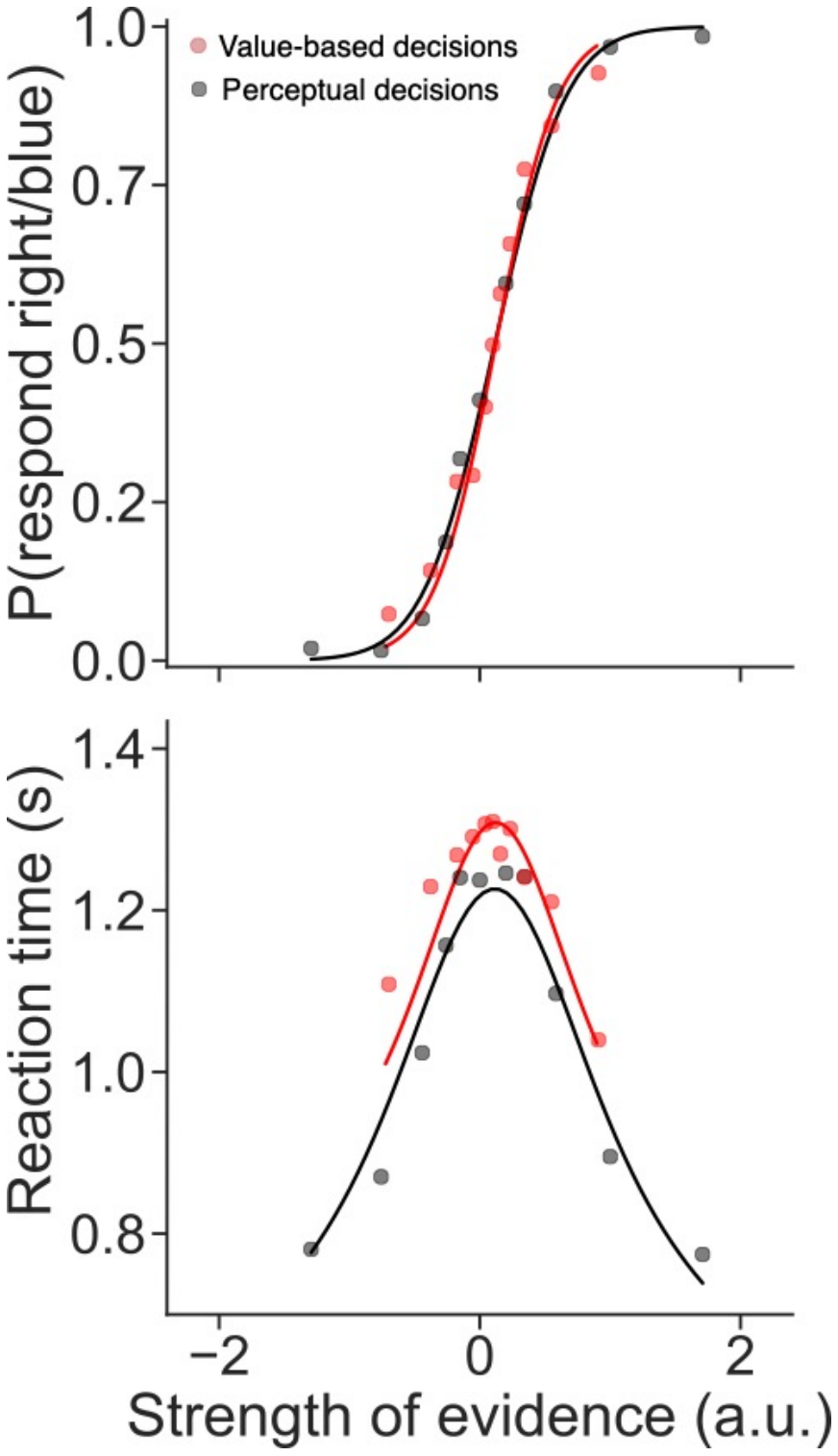

Figure 2—figure supplement 2: Comparison of data and fits from Figure 2 after rescaling the units of evidence. The *ΔValue* was transformed by scaling plus a constant such that logistic fits of the choice functions on the perceptual (black) and value tasks (red) were matched. The data and fits to drift diffusion, shown here, are identical to those in **Figure 2** except for the transformation of Δ*Value*.

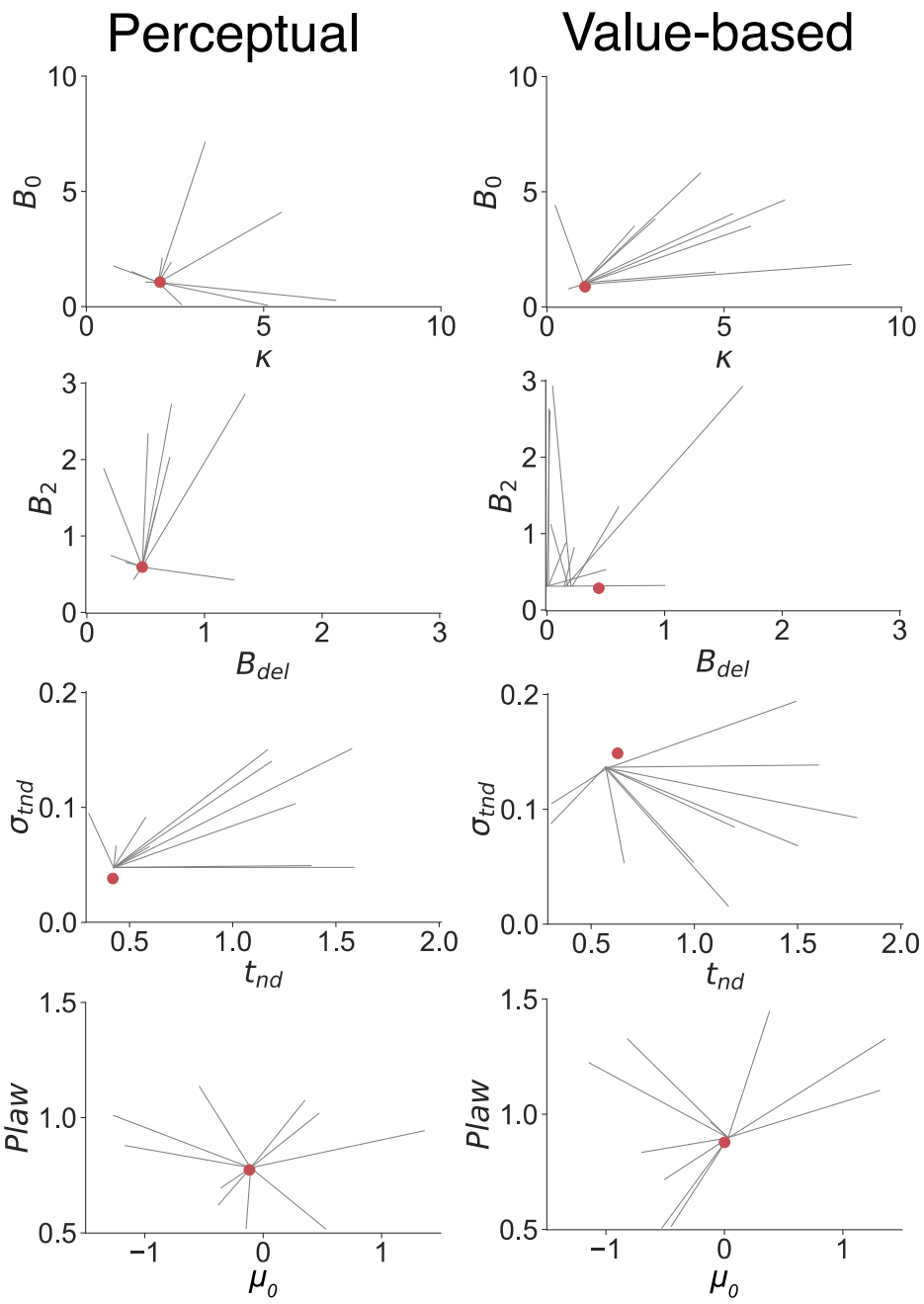

Figure 2—figure supplement 3: Parameter recovery analysis. The 8-parameter drift-diffusion model fit to the data in Figure 2 (main text) may settle on local minima. For this reason, we report the best of 100 fits using initial parameter vectors spanning ranges displayed on the axes shown here. The 8 parameters of the best fits are represented by the red dots in the four graphs in the left and right columns (Perceptual and Value based fits, as indicated. Red dot values are provided in **Figure 2—source data 1** for ALL participants). These are 2D projections of the 8D fits. Here we repeat the procedure another 10 times by performing 1000 fits to simulated data with random starting vectors using uniformly distributed elements around the reported best fits. Axes represent the range of the uniform distributions from which initial starting values were sampled. For each set of 100 fits to the simulated data, we took the best fit, thereby mimicking the procedure used to obtain fits to the actual data (see Methods). Grey lines represent the ten starting points (end of lines further from the red dot) and the corresponding best fit parameter values (end of lines nearer the red dot). The exercise recovers the fit parameters (red dots), with the following exceptions. There is a systematic offset of the standard deviation of the non-decision time (σ_{tnd}) and/or the t_{nd} in the recovered simulated data, which probably reflects a difference in the simulated data set. The failure to recover the terms governing the dynamics of bound collapse (B_2 and B_{del}; Value-based only) is a sign of over-fitting.

	Participant #	κ	B_0	B_{del}	B_2	t_{nd}	σ_{tnd}	μ_0	*Plaw*	NLL	R^2 choices	R^2 RT
Perceptual Decisions	ALL	2.08	1.06	0.47	0.59	0.42	0.04	-0.12	0.77	50879.17	0.42	0.19
	Y01	2.30	1.03	0.79	0.79	0.44	0.05	-0.20	0.79	1596.92	0.47	0.26
	Y02	4.45	1.21	0.41	2.07	0.39	0.04	-0.30	0.80	1538.29	0.66	0.35
	Y03	5.90	0.84	0.95	1.05	0.64	0.14	-0.06	1.15	1662.12	0.56	0.27
	Y04	1.89	0.67	0.69	1.05	0.60	0.07	0.06	0.83	1672.62	0.31	0.12
	Y05	2.26	0.53	2.52	0.56	0.50	0.04	0.23	0.85	1585.52	0.39	0.06
	Y06	2.98	1.15	0.52	1.43	0.43	0.01	-0.04	0.83	1642.88	0.40	0.44
	Y07	5.90	0.86	0.26	2.47	0.53	0.07	0.03	1.05	1536.25	0.54	0.40
	Y08	2.32	0.85	0.44	0.93	0.54	0.02	0.11	0.84	1638.90	0.50	0.18
	Y09	3.11	1.06	1.32	2.42	0.57	0.00	-0.26	0.73	1654.41	0.58	0.30
	Y10	2.70	1.30	0.76	1.33	0.53	0.08	-0.19	0.84	1671.78	0.57	0.35
	Y11	2.99	1.21	0.51	1.00	0.39	0.00	0.12	0.85	1643.52	0.51	0.39
	Y12	3.26	1.10	0.56	0.49	0.46	0.00	-0.35	0.81	1617.93	0.60	0.27
	Y13	4.77	0.54	3.15	0.62	0.53	0.05	-0.50	0.62	1491.64	0.55	0.11
	Y14	3.45	1.49	0.58	1.17	0.54	0.09	-0.05	0.94	1666.86	0.49	0.45
	Y15	2.31	1.03	1.30	1.48	0.39	0.00	0.17	0.79	1671.39	0.61	0.18
	Y16	2.90	1.31	0.57	1.03	0.44	0.05	-0.16	0.80	1662.57	0.51	0.42
	Y17	2.32	1.27	0.71	1.48	0.38	0.01	-0.28	0.68	1706.11	0.35	0.24
	Y18	2.50	0.98	1.12	1.62	0.53	0.05	-0.29	0.84	1644.67	0.46	0.29
	Y19	2.99	1.12	0.51	1.13	0.39	0.00	-0.32	0.73	1607.63	0.52	0.25
	Y20	2.59	1.29	1.07	1.62	0.49	0.01	-0.08	0.82	1696.64	0.56	0.35
	Y21	1.20	0.83	0.92	0.62	0.54	0.04	-0.25	0.99	1643.94	0.25	0.06
	Y22	2.61	1.36	0.66	1.07	0.39	0.01	-0.18	0.83	1641.64	0.57	0.45
	Y23	1.60	0.80	1.14	2.74	0.48	0.05	0.31	0.81	1627.51	0.41	0.05
	Y24	1.27	1.01	0.45	0.98	0.63	0.05	0.33	0.89	1715.10	0.31	0.13
	Y25	2.05	0.75	1.19	2.15	0.57	0.13	-0.18	0.73	1727.80	0.42	0.06
	Y26	2.88	1.04	0.41	0.90	0.65	0.14	-0.01	0.74	1688.56	0.47	0.23
	Y27	1.66	1.32	0.01	0.58	0.59	0.19	-0.06	0.68	1613.42	0.27	0.07
	Y28	2.20	1.67	0.80	1.42	0.34	0.00	-0.05	0.77	1701.94	0.53	0.28
	Y29	1.58	1.03	0.63	0.73	0.47	0.03	-0.23	1.27	1706.51	0.45	0.15
	Y30	3.64	1.16	0.51	0.98	0.57	0.11	0.04	0.84	1683.66	0.52	0.35
Value-based Decisions	ALL	1.07	0.88	0.44	0.29	0.63	0.15	0.00	0.88	54129.45	0.13	0.02
	Y01	1.71	0.85	0.61	0.41	0.76	0.18	0.02	0.75	1789.00	0.20	0.08
	Y02	1.59	0.62	0.16	0.51	0.72	0.11	-0.17	0.83	1712.82	0.09	0.06
	Y03	0.66	1.00	0.37	0.41	0.78	0.09	-0.19	1.15	1822.62	0.13	0.00
	Y04	1.07	0.86	1.93	3.00	0.52	0.16	0.04	0.91	1789.53	0.14	0.05
	Y05	0.71	0.58	1.14	1.20	0.58	0.07	0.14	1.14	1710.60	0.13	0.02
	Y06	0.81	0.70	0.18	1.09	0.82	0.09	-0.20	1.05	1694.36	0.06	0.08
	Y07	1.01	0.46	1.07	0.34	0.63	0.07	-0.19	0.73	1649.64	0.03	0.00
	Y08	1.64	0.80	1.47	1.35	0.63	0.04	0.02	1.16	1801.82	0.02	0.03
	Y09	1.29	0.82	0.08	0.37	0.63	0.15	0.15	0.78	1788.91	0.05	0.01
	Y10	1.61	0.89	1.04	1.12	0.88	0.14	-0.03	0.73	1802.01	0.17	0.03
	Y11	2.24	1.47	1.19	1.30	0.44	0.00	-0.02	1.22	1803.41	0.24	0.15
	Y12	1.35	0.84	0.57	0.64	0.60	0.03	0.07	0.82	1757.68	0.22	0.02
	Y13	2.15	1.08	0.26	0.67	0.70	0.04	0.04	0.84	1755.92	0.28	0.07
	Y14	0.79	1.00	0.05	0.52	0.81	0.20	-0.28	0.81	1787.96	0.07	0.02
	Y15	0.76	0.84	2.10	2.61	0.57	0.08	-0.15	1.26	1742.48	0.13	0.03
	Y16	1.30	1.24	0.37	0.49	0.71	0.20	-0.10	0.63	1772.82	0.18	0.03
	Y17	1.41	0.77	0.38	0.25	0.75	0.13	0.16	0.89	1791.70	0.17	0.02
	Y18	2.01	0.96	0.67	0.41	0.64	0.04	-0.05	1.30	1773.53	0.09	0.01
	Y19	1.29	0.80	0.99	0.73	0.57	0.08	0.18	1.23	1794.94	0.12	0.03
	Y20	0.86	1.28	0.33	0.54	0.63	0.09	-0.07	1.26	1798.79	0.16	0.03
	Y21	0.90	0.59	1.50	1.28	0.55	0.09	-0.19	0.85	1686.70	0.13	0.03
	Y22	1.47	0.73	0.03	0.29	0.89	0.16	-0.01	0.91	1764.20	0.13	0.02
	Y23	1.20	0.75	1.43	1.41	0.53	0.09	0.01	0.82	1756.52	0.14	0.08
	Y24	3.89	0.63	0.42	0.93	0.66	0.07	0.03	1.26	1704.25	0.10	0.15
	Y25	1.47	0.85	1.11	0.52	0.71	0.15	0.04	0.82	1783.27	0.24	0.09
	Y26	1.30	1.89	0.34	0.82	0.51	0.02	0.01	0.96	1772.17	0.27	0.09
	Y27	1.17	0.84	0.74	0.36	0.83	0.19	-0.23	0.76	1628.57	0.13	0.01
	Y28	2.21	0.87	0.56	0.81	0.59	0.00	-0.14	0.75	1779.80	0.10	0.04
	Y29	1.98	1.19	0.16	0.47	0.54	0.00	0.02	0.83	1793.20	0.18	0.09
	Y30	1.30	0.71	1.32	0.74	0.97	0.18	-0.22	0.90	1781.97	0.18	0.02

Figure 2—source data 1: Parameter estimates and goodness of fit measures for Experiment 1.
κ is the drift rate. B_0 is the initial height of the bound. B_{del} is the delay before the bound starts decreasing. B_2 is the coefficient of the exponential term that governs the bound decrease. t_{nd} is the non-decision time. σ_{tnd} is the standard deviation of the non-decision time. μ_0 is the bias in drift rate. *Plaw* is the coefficient of the power law applied to the stimulus strength (color coherence for perceptual and Δ*Value* for value-based). *NLL* is negative log-likelihood of the parameters given the choice and RT data. R^2 *choices* is the McFadden pseudo-R^2 for choice data given color coherence (for perceptual) or Δ*Value* (for value-based). R^2 *RT* is the R^2 for RT data given color coherence (for perceptual) or Δ*Value* (for value-based).

Figure 2—source data 2: Trial-level data for the perceptual task in Experiment 1. The file contains seven columns; subject ID, signed color coherence, p_{blue}, response (‘3#’ = left, ‘4$’ = right), reaction time, button order (1 means blue requires a left response, 2 means blue requires a right response), and whether the participant chose blue.

Figure 2—source data 3: Trial-level data for the value-based task in Experiment 1. The file contains eight columns; subject ID, reaction time, whether the participant chose the item on the right side of the screen, the value placed on the item on the left side of the screen, the value placed on the item on the right side of the screen, the name of the image that appeared on the left, the name of the image that appeared on the right, and the participant’s response (‘3#’ = left, ‘4$’ = right).

Figure 2—source code: Jupyter notebook with analysis code and output for analyses performed on data from Experiment 1.

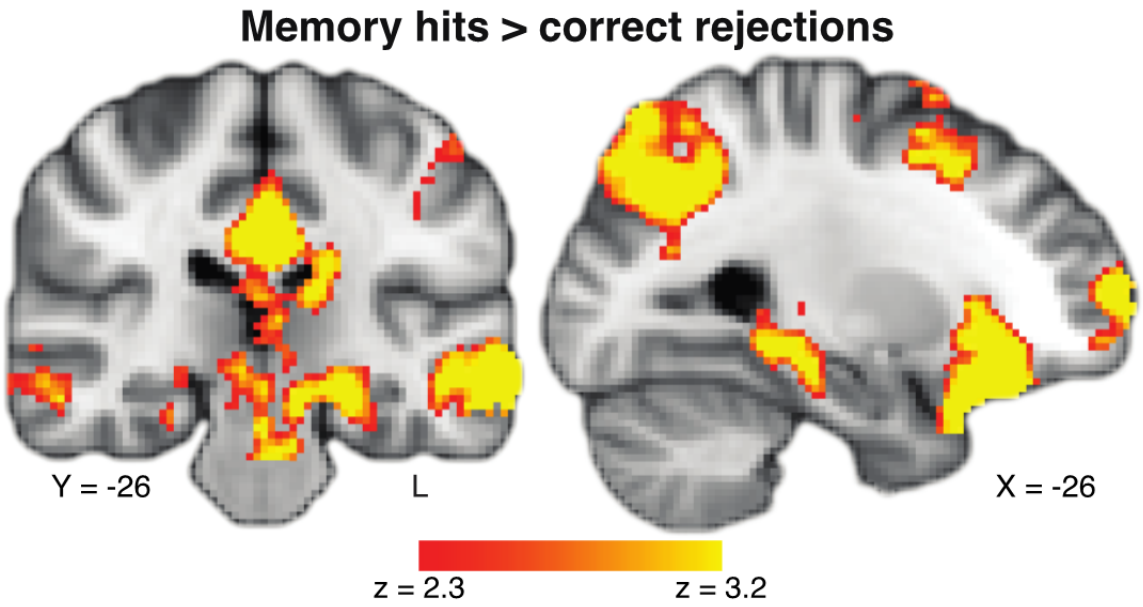

Figure 3—figure supplement 1: Parametric map of main effect of hits versus correct rejections during memory recognition. This map was used in the conjunction map presented in **Figure 3**. Coordinates reported in standard MNI space. Heatmap color bars range from z-stat = 2.3 to 3.2. The map was cluster corrected for familywise error rate at a whole-brain level with an uncorrected cluster-forming threshold of z = 2.3 and corrected extent threshold of $p < 0.05$. To see the full uncorrected map, go to https://neurovault.org/collections/BOWMEEOR/images/56726.

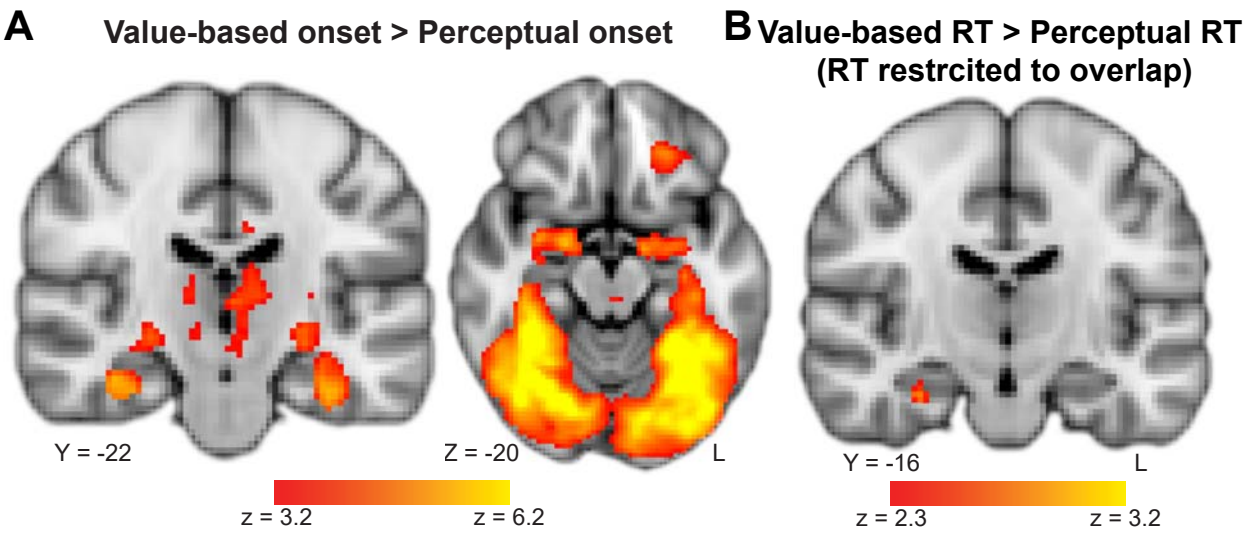

Figure 3—figure supplement 2: A) Main effect of task type on whole-brain BOLD activity at stimulus onset. We find very strong ventral stream and hippocampus activation for the value-based compared to the perceptual decision task. This is not surprising as ventral stream activity is crucial to recognition of objects such as the food items used. To see the full uncorrected map, go to https://neurovault.org/collections/BOWMEEOR/images/56728**. B)** Modulated effect of value-based compared to perceptual RT on whole-brain BOLD activity, restricted to the range of RTs that overlap across the two tasks. Even when restricting the range in RT to be equivalent across value-based and perceptual decision tasks, we still observed a more positive relationship between BOLD in the hippocampus and RT during value-based when compared to perceptual decisions, confirming the results from a simpler model in **Figure 3** and a more complex model in **Figure 3—figure supplement 3C**. To see the full uncorrected map, go to https://neurovault.org/collections/BOWMEEOR/images/56729. Coordinates reported in standard MNI space. Heatmap color bars range from z-stat = 3.2 to 6.2 in (**A**) and z-stat = 2.3 to 3.2 in (**B**). These maps were cluster-corrected at a whole-brain level $p < 0.05$.

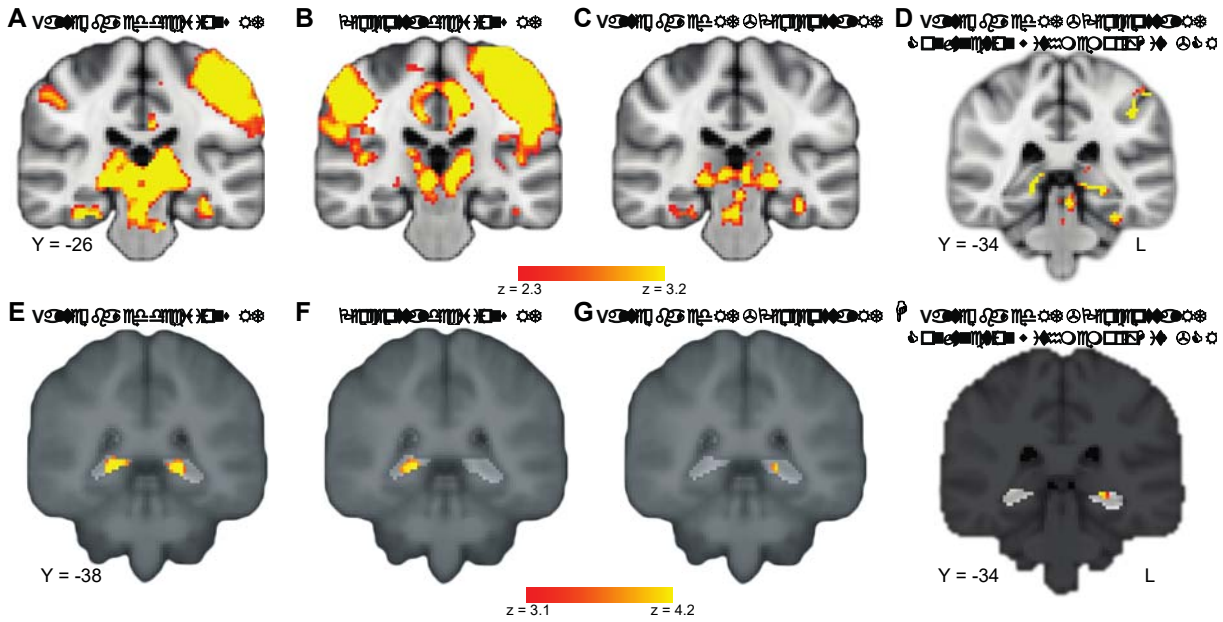

Figure 3—figure supplement 3: Parametric maps of the modulated effect of RT on BOLD in **A)** value-based (to see the full uncorrected map, go to https://neurovault.org/collections/BOWMEEOR/images/56731) and **B)** perceptual decisions (to see the full map, go to https://neurovault.org/collections/BOWMEEOR/images/56732) separately in a model that includes several regressors (e.g. mean of pair values, see *Methods*.) **C)** The contrast between maps in (**A**) and (**B**) (to see the full map, go to https://neurovault.org/collections/BOWMEEOR/images/56730). **D)** conjunction of the contrast in panel C and the memory contrast of Hits > Correct rejections**.** Coordinates reported in standard MNI space. Heatmap color bars for **A-D** range from z-stat = 2.3 to 3.2. Maps in **A-D** were cluster corrected for familywise error rate at a whole-brain level with an uncorrected cluster-forming threshold of z = 2.3 and corrected extent threshold of p < 0.05. Parametric maps of the modulated effect of RT on hippocampal BOLD in **E)** value-based (same as **A**) and **F)** perceptual decisions (same as **B**) separately. **G)** The contrast between maps in **A** and **B** (same as **C**). **H)** The same conjunction as in **D**. Heatmap color bars for **E-H** range from z-stat = 3.1 to 4.2. Maps in **E-H** were small-volume corrected within an anatomical mask of bilateral hippocampus with a voxel-level threshold of p < 0.05.

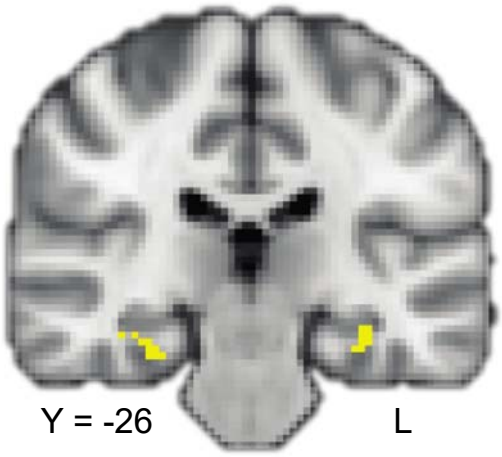

Figure 3—figure supplement 4: Timing of value-based decisions is related to activation in memory-localized regions of the hippocampus. Three-way conjunction between the map of $RT_{value\text{-}based} > RT_{perceptual}$, and two meta-analysis maps downloaded from neurosynth.org based on the terms “autobiographical memory” and “recollection”. Highlighted voxels crossed the statistical threshold in all three maps corrected for multiple comparisons.

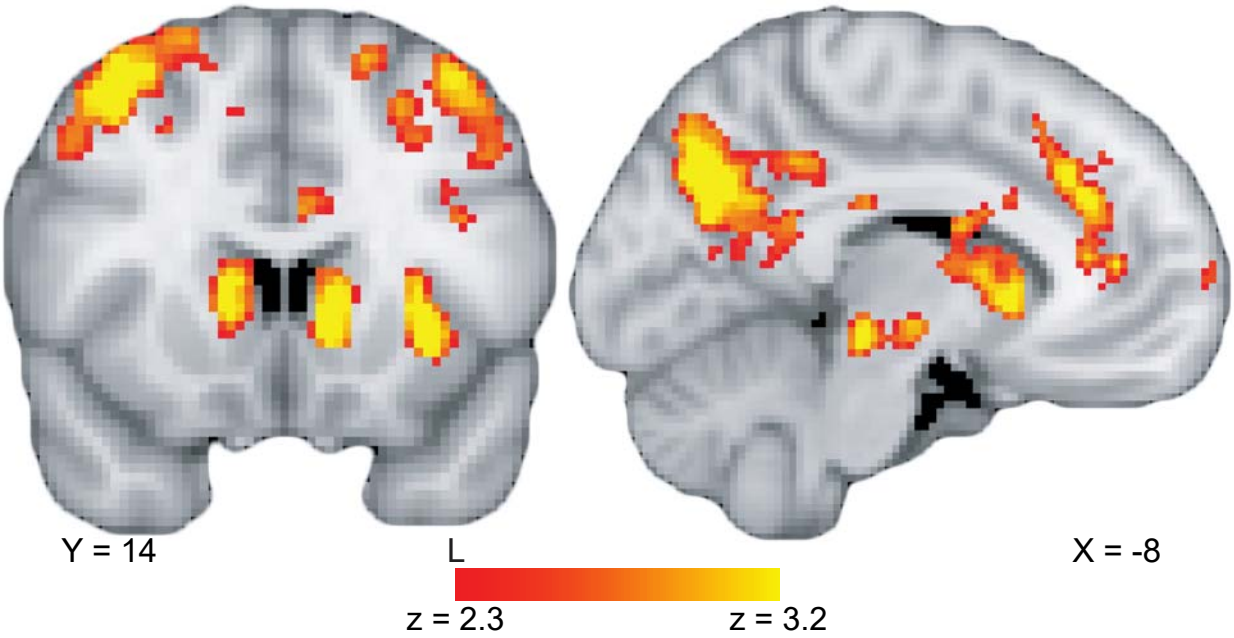

Figure 3—figure supplement 5: Value-coding brain regions. Modulated effect of the value of the chosen food. Positive values indicate a more positive relationship between the value of the chosen item and BOLD. To see the full uncorrected map, go to https://neurovault.org/collections/BOWMEEOR/images/125281. Coordinates reported in standard MNI space. Heatmap color bars range from z-stat = 2.3 to 3.2. The map was cluster corrected for familywise error rate at a whole-brain level with an uncorrected cluster-forming threshold of z = 2.3 and corrected extent threshold of $p < 0.05$.

Cluster #	Region	# voxels in region	# voxels in cluster	x	y	z	peak Z
1	L Middle Frontal Gyrus	345	514	-42	30	10	4.08
	L Inferior Frontal Gyrus, pars triangularis	93					
	L Inferior Frontal Gyrus, pars opercularis	11					
2	R Precuneous Cortex	260	382	20	-66	24	4.61
	R Intracalcarine Cortex	29					
	R Supracalcarine Cortex	19					
	R Cuneal Cortex	16					
3	L Precuneous Cortex	169	347	-14	-68	12	4.75
	L Intracalcarine Cortex	65					
	L Supracalcarine Cortex	32					
	L Cuneal Cortex	27					
4	L Intracalcarine Cortex	73	172	-8	-82	4	3.5
	L Lingual Gyrus	56					
5	L Temporal Fusiform Cortex, posterior division	63	89	-34	-42	-22	3.72
	Left Hippocampus	14					
6	Left Hippocampus	29	68	-18	-32	-2	4.22
	Left Thalamus	19					

Figure 3—source data 1: Activation table for map in Figure 3; conjunction between RT effect on BOLD for value-based greater than perceptual with effect of successful memory recognition.

Cluster #	Region	# voxels in region	# voxels in cluster	x	y	z	peak Z
1	L Lateral Occipital Cortex, superoir division	2992	35963	-36	-78	44	6
	L Frontal Pole	2729					
	L Middle Frontal Gyrus	1860					
	R Precuneous Cortex	1791					
	R Lateral Occipital Cortex, superoir division	1789					
	L Precuneous Cortex	1604					
	L Frontal Orbital Cortex	1057					
	R Cingulate Gyrus, posterior division	1025					
	L Superior Frontal Gyrus	863					
	L Paracingulate Gyrus	860					
	L Cingulate Gyrus, posterior division	860					
	Left Thalamus	759					
	L Angular Gyrus	623					
	L Supramarginal Gyrus, posterior division	540					
	Brain-Stem	456					
	L Lingual Gyrus	422					
	L Superior Parietal Lobule	416					
	Left Caudate	383					
	L Inferior Frontal Gyrus, pars triangularis	357					
	Right Thalamus	355					
	L Intracalcarine Cortex	322					
	Right Caudate	294					
	L Cingulate Gyrus, anterior division	289					
	L Inferior Frontal Gyrus, pars opercularis	275					
	Left Hippocampus	265					
	R Lingual Gyrus	245					
	L Frontal Operculum Cortex	231					
	R Paracingulate Gyrus	227					
	L Precentral Gyrus	216					
	R Intracalcarine Cortex	208					
	L Insular Cortex	197					
	L Cuneal Cortex	197					
	R Cuneal Cortex	197					
	L Postcentral Gyrus	192					
	R Cingulate Gyrus, anterior division	189					
	R Superior Parietal Lobule	171					
	R Superior Frontal Gyrus	169					
	R Angular Gyrus	168					
	R Supramarginal Gyrus, posterior division	164					
	L Subcallosal Cortex	112					
	R Frontal Pole	91					
	L Supramarginal Gyrus, anterior division	89					
	L Temporal Fusiform Cortex, posterior division	87					
	L Temporal Pole	86					
	R Juxtapositional Lobule Cortex	80					
	L Juxtapositional Lobule Cortex	78					
	L Parahippocampal Gyrus, posterior division	77					
	Left Accumbens	76					
	R Frontal Orbital Cortex	73					
	L Occipital Pole	62					
	L Frontal Medial Cortex	59					
	R Subcallosal Cortex	56					
	Right Hippocampus	56					
	L Supracalcarine Cortex	54					
	R Supracalcarine Cortex	45					
	Left Pallidum	24					
	Right Accumbens	22					
	R Parahippocampal Gyrus, posterior division	16					
	Left Putamen	12					
	L Central Opercular Cortex	11					
2	L Middle Temporal Gyrus, posterior division	893	2038	-66	-26	-4	5.6
	L Inferior Temporal Gyrus, temporooccipital part	259					
	L Middle Temporal Gyrus, temporooccipital part	246					
	L Superior Temporal Gyrus, posterior division	239					
	L Lateral Occipital Cortex, inferior division	50					
	L Inferior Temporal Gyrus, posterior division	43					
	L Middle Temporal Gyrus, anterior division	42					
	L Superior Temporal Gyrus, anterior division	21					
3	R Middle Frontal Gyrus	512	705	40	10	50	3.73
	R Precentral Gyrus	65					
	R Inferior Frontal Gyrus, pars opercularis	13					
4	R Middle Temporal Gyrus, posterior division	471	693	70	-18	-14	3.58
	R Middle Temporal Gyrus, temporooccipital part	53					
	R Superior Temporal Gyrus, posterior division	26					
	R Inferior Temporal Gyrus, temporooccipital part	15					
5	R Lingual Gyrus	31	684	12	-64	-14	3.96
6	R Frontal Pole	183	661	56	20	4	3.65
	R Inferior Frontal Gyrus, pars triangularis	92					
	R Frontal Orbital Cortex	84					
	R Insular Cortex	82					
	R Inferior Frontal Gyrus, pars opercularis	38					
	R Frontal Operculum Cortex	28					
	R Temporal Pole	15					

Figure 3—source data 2: Activation table for map in Figure 3—figure supplement 1; successful memory retrieval: hits > correct rejections.

Cluster #	Region	# voxels in region	# voxels in cluster	x	y	z	peak Z
1	R Lateral Occipital Cortex, superoir division	3635	53545	10	-80	4	7.96
	L Lateral Occipital Cortex, superoir division	3277					
	R Lingual Gyrus	1777					
	R Occipital Pole	1765					
	L Middle Frontal Gyrus	1660					
	L Occipital Pole	1640					
	L Lingual Gyrus	1405					
	R Precuneous Cortex	1322					
	L Lateral Occipital Cortex, inferior division	1268					
	R Lateral Occipital Cortex, inferior division	1211					
	L Precentral Gyrus	1013					
	L Occipital Fusiform Gyrus	926					
	R Occipital Fusiform Gyrus	880					
	Left Thalamus	820					
	R Temporal Occipital Fusiform Cortex	796					
	R Intracalcarine Cortex	770					
	R Cuneal Cortex	725					
	L Superior Frontal Gyrus	710					
	L Precuneous Cortex	680					
	L Temporal Occipital Fusiform Cortex	648					
	L Intracalcarine Cortex	631					
	Left Hippocampus	619					
	Right Thalamus	612					
	L Frontal Pole	580					
	L Superior Parietal Lobule	568					
	L Temporal Fusiform Cortex, posterior division	545					
	L Inferior Temporal Gyrus, temporooccipital part	489					
	L Cuneal Cortex	486					
	Brain-Stem	466					
	Right Hippocampus	463					
	R Cingulate Gyrus, posterior division	403					
	R Inferior Temporal Gyrus, temporooccipital part	354					
	L Cingulate Gyrus, posterior division	304					
	L Paracingulate Gyrus	291					
	R Temporal Fusiform Cortex, posterior division	284					
	Left Amygdala	277					
	L Frontal Orbital Cortex	250					
	R Superior Parietal Lobule	248					
	Right Amygdala	244					
	L Postcentral Gyrus	212					
	Left Putamen	193					
	R Supracalcarine Cortex	189					
	L Inferior Frontal Gyrus, pars triangularis	188					
	L Juxtapositional Lobule Cortex	178					
	L Inferior Frontal Gyrus, pars opercularis	174					
	R Parahippocampal Gyrus, anterior division	162					
	L Supramarginal Gyrus, anterior division	149					
	L Insular Cortex	139					
	R Paracingulate Gyrus	135					
	L Parahippocampal Gyrus, anterior division	128					
	L Parahippocampal Gyrus, posterior division	128					
	R Superior Frontal Gyrus	115					
	R Parahippocampal Gyrus, posterior division	115					
	L Cingulate Gyrus, anterior division	87					
	R Juxtapositional Lobule Cortex	77					
	R Cingulate Gyrus, anterior division	74					
	L Supracalcarine Cortex	71					
	L Central Opercular Cortex	68					
	R Angular Gyrus	60					
	L Supramarginal Gyrus, posterior division	59					
	L Inferior Temporal Gyrus, posterior division	58					
	L Angular Gyrus	40					
	Left Pallidum	34					
	Right Putamen	19					
2	R Middle Frontal Gyrus	1430	2506	36	-6	46	4.29
	R Precentral Gyrus	285					
	R Inferior Frontal Gyrus, pars triangularis	44					
	R Frontal Pole	32					
	R Superior Frontal Gyrus	15					

Figure 3—source data 3: Activation table for map in Figure 3—figure supplement 2A; overall main effect of value-based greater than perceptual decisions.

Cluster #	Region	# voxels in region	# voxels in cluster	x	y	z	peak Z
1	R Temporal Occipital Fusiform Cortex	491	4896	-30	-54	-6	5.41
	L Temporal Occipital Fusiform Cortex	476					
	L Lingual Gyrus	430					
	R Lingual Gyrus	409					
	L Intracalcarine Cortex	357					
	L Occipital Pole	295					
	R Intracalcarine Cortex	291					
	L Occipital Fusiform Gyrus	234					
	L Temporal Fusiform Cortex, posterior division	198					
	L Lateral Occipital Cortex, inferior division	165					
	R Temporal Fusiform Cortex, posterior division	141					
	R Precuneous Cortex	93					
	R Occipital Fusiform Gyrus	89					
	L Precuneous Cortex	58					
	R Supracalcarine Cortex	55					
	Right Hippocampus	34					
	R Lateral Occipital Cortex, inferior division	29					
	R Parahippocampal Gyrus, posterior division	29					
	L Supracalcarine Cortex	25					
	L Inferior Temporal Gyrus, temporooccipital part	24					
	R Cuneal Cortex	19					
	L Cuneal Cortex	12					
	R Occipital Pole	12					

Figure 3—source data 4: Activation table for map in Figure 3—figure supplement 2B; the effect of RT on BOLD for value-based greater than perceptual decisions, restricted to trials for which the range in RT was matched between the two decision tasks.

Cluster #	Region	# voxels in region	# voxels in cluster	x	y	z	peak Z
	R Lateral Occipital Cortex, superoir division	3072					
	L Lateral Occipital Cortex, superoir division	2846					
	L Precentral Gyrus	2210					
	L Postcentral Gyrus	1631					
	R Frontal Pole	1446					
	R Middle Frontal Gyrus	1388					
	L Lateral Occipital Cortex, inferior division	1212					
	R Superior Frontal Gyrus	1113					
	L Occipital Pole	1108					
	R Precentral Gyrus	1086					
	L Middle Frontal Gyrus	1074					
	R Lateral Occipital Cortex, inferior division	961					
	L Superior Parietal Lobule	927					
	R Precuneous Cortex	915					
	L Occipital Fusiform Gyrus	838					
	R Paracingulate Gyrus	824					
	R Occipital Fusiform Gyrus	790					
	Left Thalamus	775					
	Brain-Stem	755					
	L Frontal Pole	745					
	R Lingual Gyrus	741					
	R Temporal Occipital Fusiform Cortex	740					
	L Superior Frontal Gyrus	689					
	Right Thalamus	679					
	R Cingulate Gyrus, anterior division	649					
	R Superior Parietal Lobule	636					
	R Occipital Pole	636					
	L Precuneous Cortex	612					
	R Intracalcarine Cortex	592					
	L Temporal Occipital Fusiform Cortex	591					
	R Juxtapositional Lobule Cortex	586					
	L Supramarginal Gyrus, anterior division	581					
	R Insular Cortex	568					
	L Lingual Gyrus	550					
	L Juxtapositional Lobule Cortex	537					
	L Paracingulate Gyrus	533					
	L Intracalcarine Cortex	517					
	L Insular Cortex	485					
	L Cingulate Gyrus, anterior division	475					
	L Temporal Fusiform Cortex, posterior division	407					
	R Inferior Temporal Gyrus, temporooccipital part	404					
1	L Inferior Temporal Gyrus, temporooccipital part	386	55269	-36	-6	50	7
	R Inferior Frontal Gyrus, pars opercularis	302					
	R Frontal Operculum Cortex	295					
	L Frontal Operculum Cortex	265					
	R Supramarginal Gyrus, posterior division	235					
	R Supramarginal Gyrus, anterior division	232					
	R Central Opercular Cortex	229					
	L Supramarginal Gyrus, posterior division	226					
	R Temporal Fusiform Cortex, posterior division	220					
	R Angular Gyrus	197					
	L Cuneal Cortex	196					
	L Central Opercular Cortex	184					
	R Frontal Orbital Cortex	179					
	Left Hippocampus	177					
	L Inferior Frontal Gyrus, pars opercularis	167					
	R Cuneal Cortex	164					
	Right Hippocampus	163					
	L Inferior Frontal Gyrus, pars triangularis	126					
	Left Caudate	123					
	R Postcentral Gyrus	121					
	R Parahippocampal Gyrus, anterior division	111					
	R Inferior Frontal Gyrus, pars triangularis	100					
	L Angular Gyrus	88					
	Left Pallidum	73					
	L Inferior Temporal Gyrus, posterior division	59					
	L Frontal Orbital Cortex	57					
	L Cingulate Gyrus, posterior division	56					
	R Parahippocampal Gyrus, posterior division	53					
	R Supracalcarine Cortex	51					
	L Parahippocampal Gyrus, anterior division	47					
	L Supracalcarine Cortex	40					
	R Middle Temporal Gyrus, temporooccipital part	31					
	Left Putamen	31					
	R Cingulate Gyrus, posterior division	28					
	Right Amygdala	28					
	Left Amygdala	25					
	L Middle Temporal Gyrus, temporooccipital part	22					
	R Temporal Pole	22					
	R Heschl's Gyrus (includes H1 and H2)	15					
	L Parahippocampal Gyrus, posterior division	14					
	R Temporal Fusiform Cortex, anterior division	12					
	R Inferior Temporal Gyrus, posterior division	10					

Figure 3—source data 5: Activation table for map in Figure 3—figure supplement 3A; effect of value-based RT on BOLD.

Cluster #	Region	# voxels in region	# voxels in cluster	x	y	z	peak Z
	L Precentral Gyrus	3111					
	R Lateral Occipital Cortex, superoir division	2731					
	L Postcentral Gyrus	2545					
	L Lateral Occipital Cortex, superoir division	2259					
	R Precentral Gyrus	2108					
	L Lateral Occipital Cortex, inferior division	1553					
	R Lateral Occipital Cortex, inferior division	1496					
	L Superior Parietal Lobule	1396					
	R Postcentral Gyrus	1248					
	R Superior Parietal Lobule	1200					
	R Occipital Fusiform Gyrus	849					
	L Occipital Fusiform Gyrus	843					
	L Occipital Pole	818					
	R Frontal Pole	771					
	R Occipital Pole	746					
	R Superior Frontal Gyrus	741					
	R Juxtapositional Lobule Cortex	737					
	R Cingulate Gyrus, anterior division	727					
	L Middle Frontal Gyrus	723					
	L Supramarginal Gyrus, anterior division	683					
	R Supramarginal Gyrus, anterior division	680					
	L Superior Frontal Gyrus	597					
	L Juxtapositional Lobule Cortex	583					
	R Middle Frontal Gyrus	560					
	L Frontal Pole	552					
	L Central Opercular Cortex	545					
	R Paracingulate Gyrus	507					
	Left Thalamus	458					
	R Temporal Occipital Fusiform Cortex	449					
	R Supramarginal Gyrus, posterior division	444					
	R Insular Cortex	437					
	Right Thalamus	433					
	L Cingulate Gyrus, anterior division	430					
	R Precuneous Cortex	417					
	L Insular Cortex	410					
	R Inferior Temporal Gyrus, temporooccipital part	381					
	L Paracingulate Gyrus	380					
	L Temporal Occipital Fusiform Cortex	369					
	R Central Opercular Cortex	364					
1	L Parietal Operculum Cortex	351	54515	-40	-12	54	6.72
	R Middle Temporal Gyrus, temporooccipital part	286					
	L Supramarginal Gyrus, posterior division	277					
	L Precuneous Cortex	253					
	R Parietal Operculum Cortex	249					
	R Frontal Operculum Cortex	246					
	R Lingual Gyrus	244					
	L Frontal Operculum Cortex	208					
	L Inferior Temporal Gyrus, temporooccipital part	195					
	R Inferior Frontal Gyrus, pars opercularis	193					
	Brain-Stem	172					
	L Cingulate Gyrus, posterior division	166					
	L Planum Temporale	165					
	L Lingual Gyrus	130					
	R Cingulate Gyrus, posterior division	118					
	Left Putamen	110					
	L Heschl's Gyrus (includes H1 and H2)	91					
	R Planum Temporale	85					
	Right Hippocampus	85					
	R Angular Gyrus	78					
	L Intracalcarine Cortex	77					
	R Heschl's Gyrus (includes H1 and H2)	75					
	Right Pallidum	73					
	R Cuneal Cortex	61					
	L Middle Temporal Gyrus, temporooccipital part	56					
	Left Hippocampus	55					
	R Frontal Orbital Cortex	54					
	L Temporal Fusiform Cortex, posterior division	48					
	L Angular Gyrus	47					
	Left Pallidum	46					
	L Frontal Orbital Cortex	42					
	R Temporal Fusiform Cortex, posterior division	41					
	L Inferior Frontal Gyrus, pars opercularis	39					
	L Planum Polare	36					
	Right Putamen	34					
	L Inferior Temporal Gyrus, posterior division	33					
	R Inferior Frontal Gyrus, pars triangularis	30					
	R Inferior Temporal Gyrus, posterior division	16					
	L Inferior Frontal Gyrus, pars triangularis	13					
	R Temporal Pole	13					

Figure 3—source data 6: Activation table for map in Figure 3—figure supplement 3B; effect of perceptual RT on BOLD.

Cluster #	Region	# voxels in region	# voxels in cluster	x	y	z	peak Z
1	L Lateral Occipital Cortex, superoir division	2149	14697	36	-42	-16	5.5
	R Lateral Occipital Cortex, superoir division	1592					
	R Temporal Occipital Fusiform Cortex	602					
	L Occipital Fusiform Gyrus	581					
	R Intracalcarine Cortex	526					
	L Temporal Occipital Fusiform Cortex	492					
	L Intracalcarine Cortex	473					
	R Lingual Gyrus	436					
	R Precuneous Cortex	432					
	Left Thalamus	420					
	L Occipital Pole	415					
	R Occipital Fusiform Gyrus	412					
	L Lingual Gyrus	371					
	Brain-Stem	338					
	L Lateral Occipital Cortex, inferior division	317					
	L Precuneous Cortex	304					
	Right Thalamus	298					
	L Superior Parietal Lobule	258					
	L Temporal Fusiform Cortex, posterior division	233					
	R Lateral Occipital Cortex, inferior division	184					
	R Temporal Fusiform Cortex, posterior division	121					
	L Cuneal Cortex	118					
	Right Hippocampus	116					
	R Cuneal Cortex	95					
	R Superior Parietal Lobule	90					
	R Inferior Temporal Gyrus, temporooccipital part	89					
	Left Hippocampus	88					
	R Parahippocampal Gyrus, anterior division	82					
	R Angular Gyrus	64					
	L Inferior Temporal Gyrus, temporooccipital part	61					
	R Occipital Pole	61					
	R Supracalcarine Cortex	49					
	L Supracalcarine Cortex	32					
	R Parahippocampal Gyrus, posterior division	31					
	L Supramarginal Gyrus, posterior division	18					
	L Angular Gyrus	16					
	L Parahippocampal Gyrus, posterior division	14					
2	R Paracingulate Gyrus	681	4755	44	16	8	4.6
	R Middle Frontal Gyrus	631					
	R Superior Frontal Gyrus	451					
	L Paracingulate Gyrus	412					
	R Insular Cortex	307					
	R Frontal Operculum Cortex	269					
	R Precentral Gyrus	208					
	L Juxtapositional Lobule Cortex (formerly Supplementary Motor Cortex)	202					
	R Juxtapositional Lobule Cortex (formerly Supplementary Motor Cortex)	147					
	R Frontal Pole	121					
	R Cingulate Gyrus, anterior division	111					
	L Superior Frontal Gyrus	101					
	R Inferior Frontal Gyrus, pars opercularis	94					
	R Frontal Orbital Cortex	87					
	L Cingulate Gyrus, anterior division	40					
	R Inferior Frontal Gyrus, pars triangularis	23					
	R Central Opercular Cortex	23					
3	L Middle Frontal Gyrus	442	1809	-52	0	28	4.09
	L Frontal Operculum Cortex	238					
	L Precentral Gyrus	233					
	L Insular Cortex	205					
	L Frontal Pole	107					
	L Inferior Frontal Gyrus, pars triangularis	93					
	L Inferior Frontal Gyrus, pars opercularis	58					
	L Frontal Orbital Cortex	18					
	L Central Opercular Cortex	11					
4	L Precentral Gyrus	259	503	-36	-6	50	3.75
	L Middle Frontal Gyrus	161					
	L Superior Frontal Gyrus	16					

Figure 3—source data 7: Activation table for map in Figure 3—figure supplement 3C; value-based RT > perceptual RT.

Contrast	Cluster #	Region	# voxels in cluster	x	y	z	peak Z
VB RT	1	Right Hippocampus	66	20	-36	0	5.71
	2	Left Hippocampus	61	-18	-38	0	5.2
	3	Right Hippocampus	12	28	-4	-28	4.26
Perceptual RT	1	Right Hippocampus	39	20	-38	0	4.54
VB RT > Perceptual RT	1	Right Hippocampus	11	20	-34	-4	3.88
	2	Left Hippocampus	10	-18	-38	0	4.09
	3	Right Hippocampus	6	28	-10	-28	3.94

Figure 3—source data 8: Activation table for map in **Figure 3—figure supplements 3E-G**.

Cluster #	Region	# voxels in region	# voxels in cluster	x	y	z	peak Z
1	L Lateral Occipital Cortex, superoir division	1683	13956	54	-38	44	4.69
	R Lateral Occipital Cortex, superoir division	1647					
	R Precuneous Cortex	1621					
	R Angular Gyrus	1176					
	L Precuneous Cortex	1128					
	R Cingulate Gyrus, posterior division	650					
	R Supramarginal Gyrus, posterior division	629					
	R Middle Temporal Gyrus, temporooccipital part	620					
	L Cingulate Gyrus, posterior division	446					
	L Supramarginal Gyrus, posterior division	406					
	L Angular Gyrus	389					
	L Superior Parietal Lobule	353					
	R Superior Parietal Lobule	242					
	R Supramarginal Gyrus, anterior division	229					
	L Supramarginal Gyrus, anterior division	218					
	R Lateral Occipital Cortex, inferior division	154					
	R Cuneal Cortex	133					
	R Middle Temporal Gyrus, posterior division	113					
	R Intracalcarine Cortex	90					
	R Inferior Temporal Gyrus, temporooccipital part	77					
	L Intracalcarine Cortex	67					
	L Cuneal Cortex	24					
	R Postcentral Gyrus	19					
	R Supracalcarine Cortex	14					
2	R Middle Frontal Gyrus	1191	5592	-40	24	36	4.48
	L Middle Frontal Gyrus	1039					
	R Superior Frontal Gyrus	363					
	L Paracingulate Gyrus	352					
	L Superior Frontal Gyrus	348					
	R Paracingulate Gyrus	295					
	Left Caudate	291					
	Right Caudate	208					
	L Cingulate Gyrus, anterior division	167					
	R Cingulate Gyrus, anterior division	138					
	L Insular Cortex	127					
	R Frontal Pole	79					
	Left Thalamus	47					
	L Precentral Gyrus	43					
	L Inferior Frontal Gyrus, pars opercularis	17					
	R Precentral Gyrus	14					
	Right Pallidum	14					
	Left Accumbens	11					
3	L Frontal Pole	583	635	-36	50	6	3.53
4	Right Thalamus	272	607	-10	-26	-8	3.56
	Brain-Stem	61					
	Left Thalamus	40					
	Left Hippocampus	32					

Figure 3—source data 9: Activation table for map in **Figure 3—figure supplement 5**: Modulated effect of the value of the chosen food.

Cluster #	Region	# voxels in region	# voxels in cluster	x	y	z	peak Z
1	R Superior Parietal Lobule	178	495	12	-48	54	3.69
	R Precuneous Cortex	143					
	R Postcentral Gyrus	71					

Figure 4—source data 1: Activation table for map in Figure 4; PPI for value-based decision trials with hippocampus seed modulated by RT.

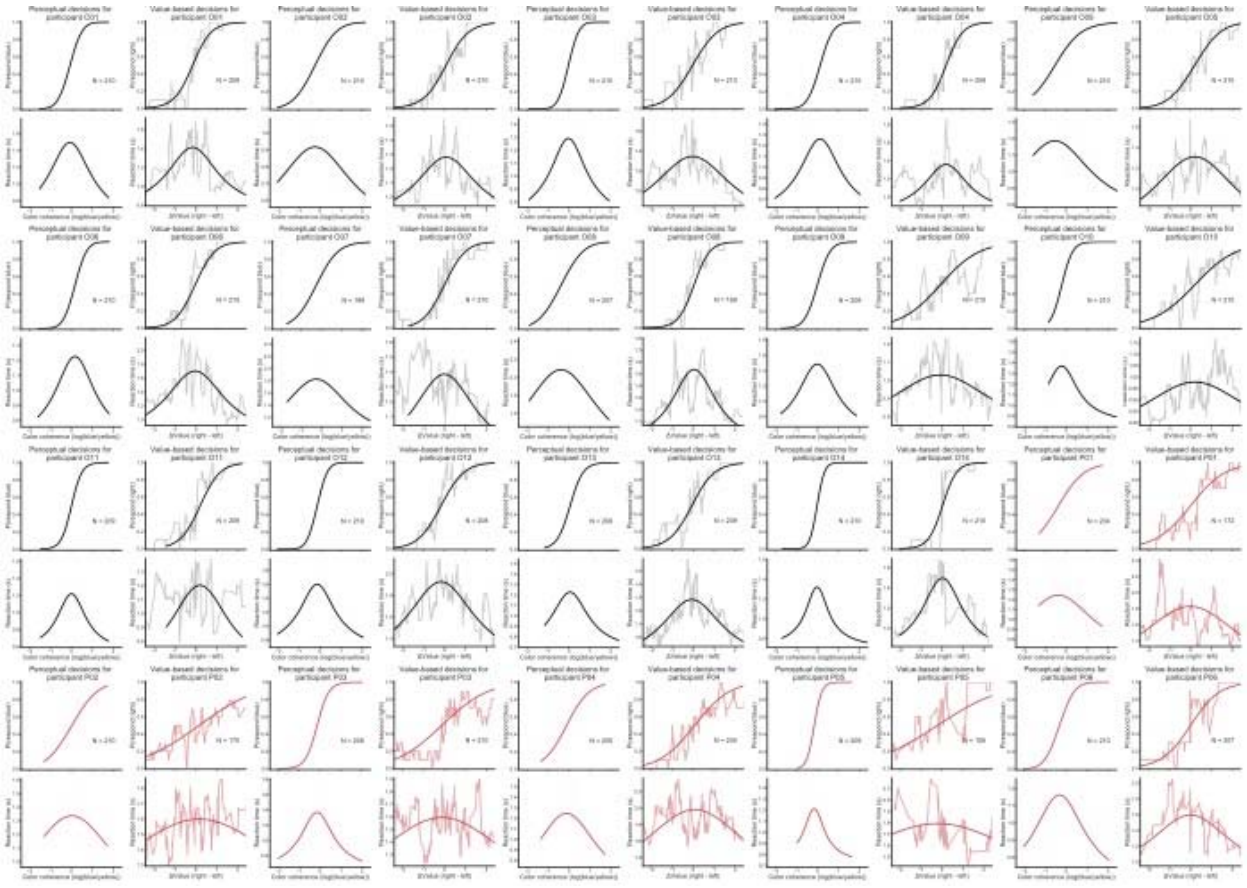

Figure 5—figure supplement 1: Data and fits for value-based and perceptual decisions per participant in Experiment 2. Light lines are running means. Dots are means and error bars are standard errors of the mean. Solid lines are model fits.

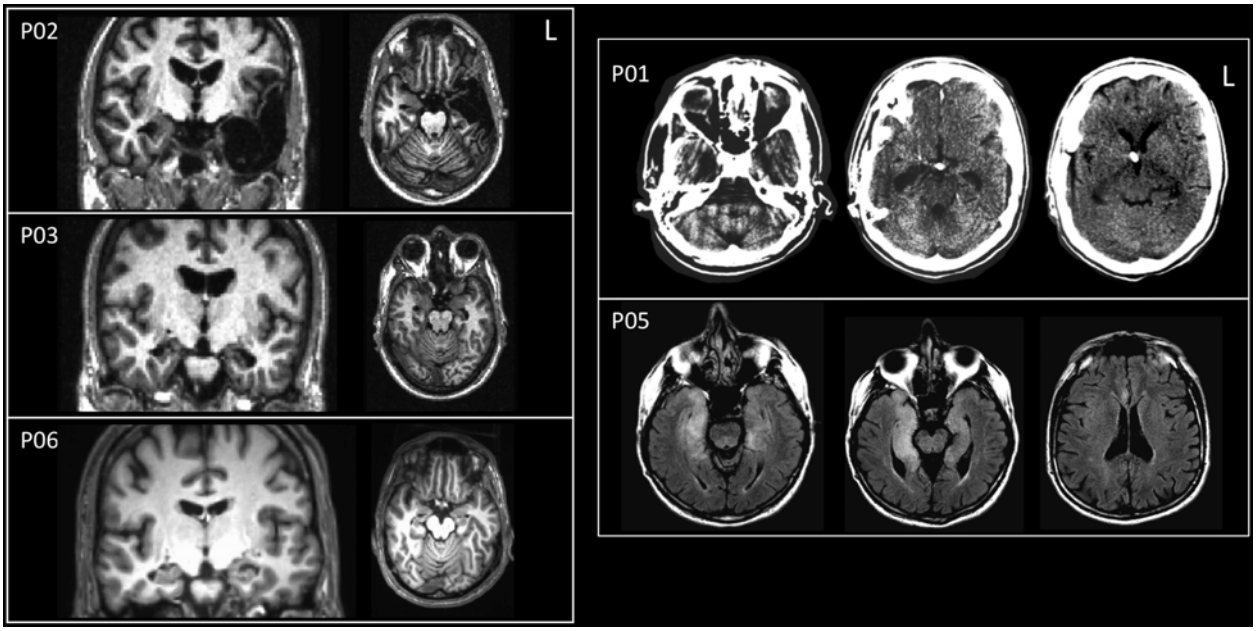

Figure 5—figure supplement 2: Brain images for five out of six amnesic patients included in experiment 2. MRI images for four patients (T1-weighted images for P02, P03, and P06, and T2-weighted images for P05 are presented), and computed tomography (CT) images for patient P01 show damage to the hippocampus in all cases. Brain images are not available for the sixth patient.

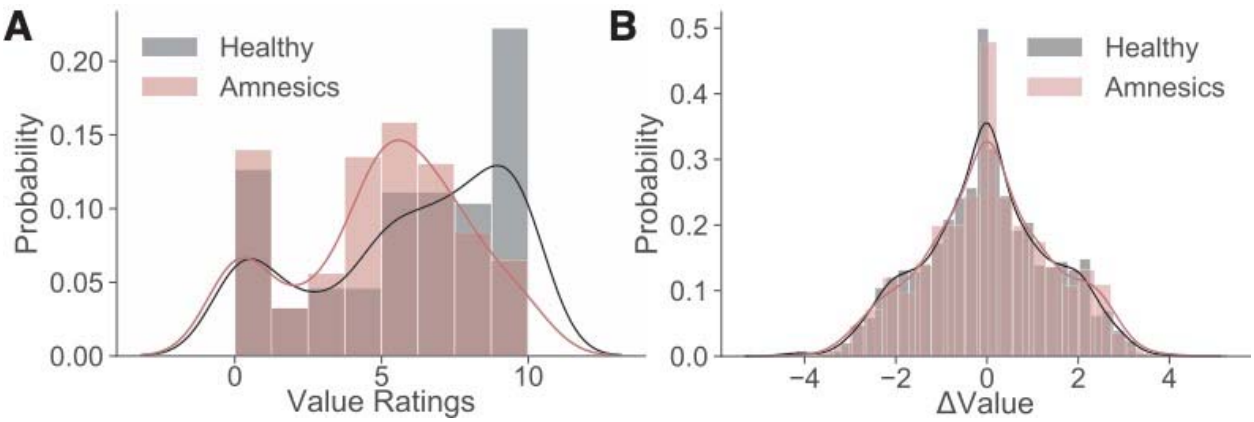

Figure 5—figure supplement 3: Distributions of value ratings and resulting *ΔValues* used during the choice phase. Probability histogram of **A)** value ratings from the rating phase and of **B)** the resulting *ΔValues* in the choice phase for healthy participants (black) and amnesic patients (red). The solid lines are univariate kernel density estimates fit to the data. Healthy controls and amnesic patients use the full range of the rating scale when valuing individual items. The resulting distribution of *ΔValues* calculated from these value ratings in both groups are largely overlapping.

Figure 5—figure supplement 4: Support for a qualitative prediction of a heuristic decision strategy in the amnesic patient group. We evaluated a heuristic model in which choices and RT were governed by a small set of items that were either strongly liked or disliked and thus induce fast "*trivial*" decisions. The remainder of "*non-trivial*" decisions are stochastic and slow, accounting for the majority of trials. The model posits that RT is not governed by Δ*Value* but by whether the comparison is *trivial* or *non-trivial*. This qualitative prediction is refuted in panels **A** and **B** (healthy participants, p<0.005), but not in panel **C** (amnesic patients; p=0.29). Fits to establish the best criterion for the *trivial/non-trivial* designation were established for each participant. Solid lines are least square fits to mean RT for choices between items, aggregated across participants. Shaded area is the bootstrapped 90% confidence interval for the regression slope estimate. Points and error bars (means ± s.e.m.) are plotted corresponding to the bins of Δ*Value* shown in other RT graphs (e.g., **Figures 2** and **5**). The dashed lines are the predictions from the best fitting heuristic model: the mean RT from all trials that the model designates as *non-trivial*. Other qualitative predictions of the model are not well supported. For example, there is no criterion on item ratings that satisfies the *trivial/non-trivial* distinction. No values of κ_1 and κ_2 identify *trivial* trials for which choices are fully consistent with the heuristic model prediction, as shown by the heat maps. Insets show the proportion of trials in which participants chose the item that should be chosen trivially, based on the heuristic. The range of potential criteria ($\kappa_{1,2}$) span the highest and lowest tertiles of the values derived from the auction (**A**) and the rating scales (**B**,**C**). The cell marked X contains no data. The heuristic model also does not explain why the patients are slow overall (especially on *trivial* decisions; not shown). The heuristic model does not outperform the drift diffusion model for any of the groups, but it highlights a qualitative distinction between the amnesic patients and the other healthy groups. See *Methods* for additional details.

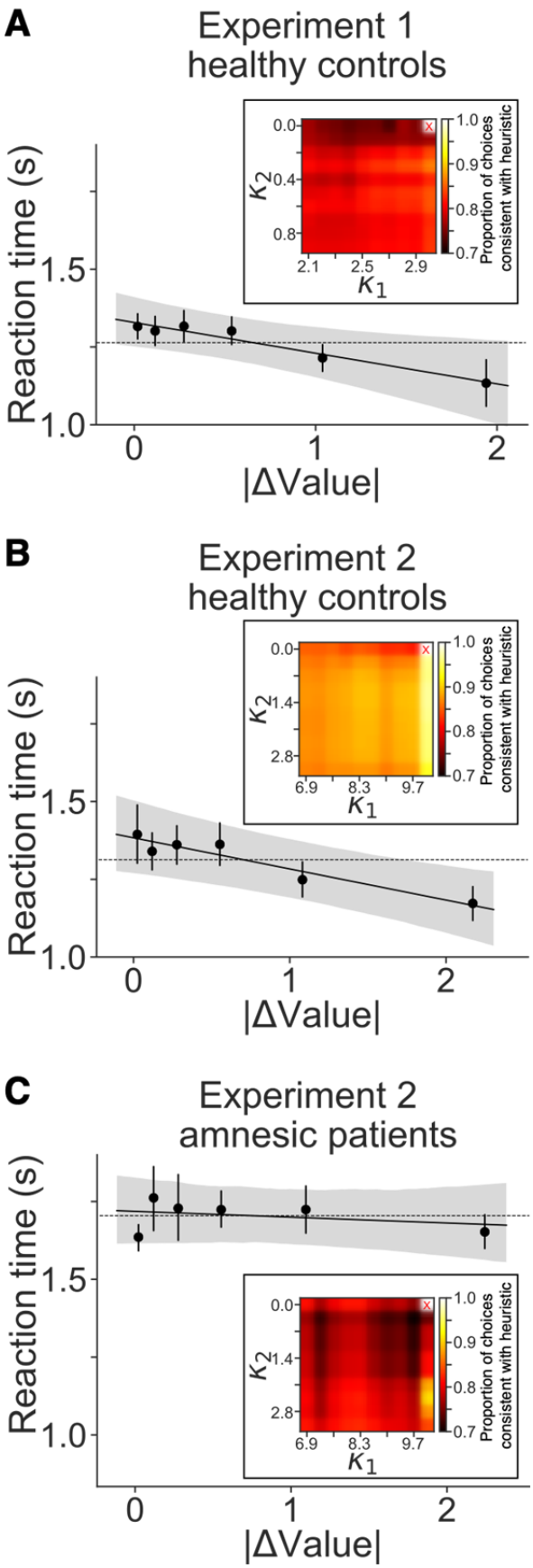

	Group	Participant #	κ	B_0	B_{del}	B_2	t_{nd}	σ_{tnd}	μ_0	*Plaw*	NLL	R^2 choices	R^2 RT
Perceptual Decisions	**Older healthy participants**	ALL O	1.49	0.91	1.59	0.60	0.57	0.13	0.09	0.81	25060.01	0.32	0.12
		O01	1.67	1.72	0.59	0.97	0.30	0.00	0.07	0.83	1753.60	0.35	0.26
		O02	1.29	1.12	0.34	1.64	0.30	0.00	0.25	1.11	1657.66	0.30	0.21
		O03	2.47	1.27	0.39	1.40	0.55	0.08	0.02	0.95	1637.78	0.51	0.40
		O04	1.83	1.21	0.33	0.64	0.41	0.06	-0.12	1.03	1712.45	0.40	0.25
		O05	1.09	0.72	1.18	0.74	0.66	0.14	0.54	1.27	1763.35	0.18	0.05
		O06	2.22	1.25	0.33	1.32	0.52	0.00	-0.17	0.85	1624.13	0.52	0.31
		O07	0.87	1.13	1.99	1.47	0.66	0.04	0.26	1.25	1758.94	0.28	0.10
		O08	0.80	2.66	0.66	0.98	0.49	0.12	0.37	0.94	1773.82	0.29	0.17
		O09	1.62	1.10	0.95	0.37	0.45	0.10	0.01	0.89	1775.49	0.48	0.18
		O10	2.48	0.80	0.93	1.12	0.77	0.06	0.22	1.40	1722.99	0.20	0.16
		O11	2.31	0.88	2.05	2.24	0.45	0.03	0.00	0.82	1697.63	0.43	0.20
		O12	2.04	1.43	0.61	0.84	0.52	0.08	0.14	1.03	1750.97	0.40	0.31
		O13	2.03	0.80	1.15	0.52	0.59	0.08	-0.06	1.35	1753.64	0.20	0.11
		O14	3.49	0.88	0.56	0.52	0.65	0.11	0.02	1.24	1687.64	0.47	0.27
	Amnesic patients	ALL P	1.45	0.80	2.42	1.89	0.59	0.14	0.20	0.83	10612.56	0.27	0.09
		P01	0.97	0.83	2.52	3.00	0.55	0.13	0.38	0.78	1771.78	0.16	0.06
		P02	0.94	1.29	0.70	2.12	0.46	0.11	-0.02	0.78	1758.10	0.18	0.10
		P03	1.93	0.94	1.61	0.36	0.50	0.07	0.14	1.00	1728.55	0.40	0.20
		P04	1.00	0.95	1.92	0.88	0.36	0.07	0.11	0.78	1798.76	0.19	0.08
		P05	3.86	0.73	1.67	1.20	0.67	0.09	0.16	0.70	1642.11	0.47	0.20
		P06	1.91	0.99	0.46	2.04	0.56	0.04	0.32	1.02	1657.65	0.42	0.21
Value-based Decisions	**Older healthy participants**	ALL O	1.11	0.85	1.47	0.43	0.64	0.12	-0.04	0.84	24342.69	0.41	0.06
		O01	1.27	0.88	0.59	0.00	0.64	0.06	0.15	0.93	1711.87	0.52	0.11
		O02	1.28	0.72	1.70	0.02	0.76	0.09	-0.07	1.01	1692.85	0.42	0.14
		O03	0.95	0.95	0.92	0.97	0.57	0.05	0.03	1.18	1746.98	0.37	0.13
		O04	1.59	0.78	1.42	0.00	0.73	0.12	-0.20	0.75	1704.86	0.55	0.04
		O05	0.84	1.26	0.54	0.77	0.36	0.03	-0.20	0.94	1757.62	0.42	0.07
		O06	1.02	1.13	0.95	0.30	0.60	0.10	0.03	1.20	1783.20	0.57	0.13
		O07	1.19	0.97	0.31	0.45	0.68	0.08	0.00	0.71	1753.40	0.32	0.03
		O08	1.55	0.89	0.74	0.22	0.79	0.14	-0.04	0.89	1381.25	0.56	0.11
		O09	0.85	0.64	0.41	0.22	0.63	0.14	0.07	1.15	1727.43	0.22	0.06
		O10	0.90	0.55	1.92	0.03	0.66	0.10	-0.20	0.98	1685.14	0.21	0.03
		O11	1.23	0.85	2.89	0.00	0.49	0.00	-0.20	0.72	1738.75	0.39	0.05
		O12	0.95	1.15	0.04	0.23	1.00	0.19	0.16	0.96	1769.01	0.53	0.09
		O13	1.23	0.74	1.03	0.02	0.72	0.13	0.06	0.95	1716.57	0.42	0.12
		O14	1.60	0.94	1.42	0.01	0.64	0.07	-0.02	0.90	1702.01	0.57	0.23
	Amnesic patients	ALL P	0.58	1.29	0.27	0.34	0.66	0.13	-0.02	0.81	9935.26	0.22	0.02
		P01	0.60	1.01	0.74	0.00	0.84	0.07	0.02	1.20	1502.96	0.35	0.03
		P02	0.38	1.13	0.16	0.35	0.75	0.14	-0.17	0.98	1497.74	0.10	0.01
		P03	0.49	1.39	0.00	0.48	0.69	0.12	0.13	0.91	1829.30	0.18	0.02
		P04	0.56	1.41	0.52	0.41	0.75	0.16	-0.07	0.89	1816.22	0.29	0.02
		P05	0.35	1.00	0.26	0.21	0.96	0.07	0.20	1.34	1360.24	0.12	0.02
		P06	0.75	0.96	0.86	0.00	0.68	0.08	0.01	1.23	1847.93	0.34	0.08

Figure 5—source data 1: Parameter estimates and goodness of fit measures for Experiment 2.
κ is the drift rate. B_0 is the initial height of the bound. B_{del} is the delay before the bound starts decreasing. B_2 is the coefficient of the exponential term that governs the bound decrease. t_{nd} is the non-decision time. σ_{tnd} is the standard deviation of the non-decision time. μ_0 is the bias in drift rate. *Plaw* is the coefficient of the power law applied to the stimulus strength (color coherence for perceptual and Δ*Value* for value-based). *NLL* is negative log-likelihood of the parameters given the choice and RT data. R^2 *choices* is the McFadden pseudo-R^2 for choice data given color coherence (for perceptual) or Δ*Value* (for value-based). R^2 *RT* is the R^2 for RT data given color coherence (for perceptual) or Δ*Value* (for value-based).

Figure 5—source data 2: Trial-level data for the perceptual task in Experiment 2. The file contains eight columns; subject ID, group (healthy or amnesia), signed color coherence, p_{blue}, response ('z' = left, 'm' = right), reaction time, button order (1 means blue requires a left response, 2 means blue requires a right response), and whether the participant chose blue.

Figure 5—source data 3: Trial-level data for the value-based task in Experiment 2. The file contains twelve columns; subject ID, group (healthy or amnesia), the name of the image that appeared on the left side of the screen, the name of the image that appeared on the right, the participant's response ('z' = left, 'm' = right), reaction time, the value rating of the item on the left, the value rating of the item on the right, whether the participant chose the item on the right side of the screen, the z-scored value rating of the item on the left, the z-scored value rating of the item on the right, and ΔValue.

Figure 5—source code: Jupyter notebook with analysis code and output for analyses performed on data from Experiment 2.